


Article

Formulation of a Jet Fuel Surrogate and Its Kinetic Chemical Mechanism by Emulating Physical and Chemical Properties of Real Jet Fuel

Guangze Li ^{1,2,3}, Boxuan Cui ¹, Chenglin Zhang ³, Liuyong Chang ^{1,2,3,*}  and Longfei Chen ^{1,*}

¹ School of Energy and Power Engineering, Beihang University, Beijing 100191, China; liguangze@buaa.edu.cn (G.L.)

² Beihang Hangzhou Innovation Institute Yuhang, Hangzhou 310023, China

³ Zhongfa Aviation Institute of Beihang University, Hangzhou 311115, China

* Correspondence: changliuyong@buaa.edu.cn (L.C.); chenlongfei@buaa.edu.cn (L.C.)

Abstract: The application of jet fuel in gas turbines and diesel engines adheres to the Army's single-fuel forward policy, streamlining supply chains. To ensure precise engine combustion numerical studies, surrogate fuels and mechanisms should faithfully replicate real fuel properties and combustion traits. In this work, a new four-component jet fuel surrogate containing 39.05% n-dodecane/21.79% isocetane/11.49% decalin/27.67% toluene by mole fraction is formulated based on a property optimizer. The new-formulated fuel surrogate can satisfactorily emulate the chemical and physical properties of real jet fuel, including cetane number (CN), threshold sooting index (TSI), molecular weight (MW), lower heating value (LHV), the ratio of hydrogen and carbon (H/C), liquid density, viscosity, and surface tension. Furthermore, a reduced and robust kinetic chemical mechanism (containing 124 species and 590 reactions) that could be directly employed in practical engine combustion simulations has also been developed for the proposed surrogate jet fuel. The mechanism is validated through comprehensive experimental data, including ignition delay time (IDT) determined in shock tubes and rapid compression machines (RCMs), species mole fractions measured in premixed flames and jet stirred reactors (JSRs), and laminar flame speeds. Generally, the property deviations of the jet fuel surrogate are less than 2% except for MW (10.73%), viscosity (5.88%), and surface tension (8.71%). The comparison results between the predictions and measurements are in good agreement, indicating that the current kinetic mechanism is capable of reflecting the oxidation process of real jet fuel. The current mechanism can accurately capture variations in the ignition delay time in the negative temperature coefficient (NTC) region as well. In the future, the proposed surrogate jet fuel could be applied in practical engine computational fluid dynamic (CFD) simulations.

Keywords: fuel property; ignition delay time; species profile; laminar flame speed; reduced chemical mechanism



check for updates

Citation: Li, G.; Cui, B.; Zhang, C.; Chang, L.; Chen, L. Formulation of a Jet Fuel Surrogate and Its Kinetic Chemical Mechanism by Emulating Physical and Chemical Properties of Real Jet Fuel. *Sustainability* **2023**, *15*, 13792. <https://doi.org/10.3390/su151813792>

Academic Editor: Talal Yusaf

Received: 7 July 2023

Revised: 4 September 2023

Accepted: 12 September 2023

Published: 15 September 2023



Copyright: © 2023 by the authors. Licensee MDPI, Basel, Switzerland. This article is an open access article distributed under the terms and conditions of the Creative Commons Attribution (CC BY) license (<https://creativecommons.org/licenses/by/4.0/>).

1. Introduction

Jet fuel has been widely adopted as a general fuel for aircraft and ground vehicles in battlefields under the auspices of the U.S. army single-fuel policy [1], which aims to significantly reduce the costs of fuel supply. Furthermore, jet fuel is expected to reduce NO_x and particle matter emissions in diesel engines, and thus it would be beneficial to investigate the effects of using jet fuel on the combustion and emission characteristics of diesel engines. However, due to the limitation of current computational capacity, the real jet fuel, which comprises hundreds of compounds, was unable to be directly employed in a practical engine simulation [2,3]. Therefore, surrogate jet fuels, which normally consist of several well-characterized compounds, were proposed [4–6]. The research on surrogate jet fuels is expected to achieve sustainability in the aviation fuel industry.

Previous research studies have been conducted on the development of jet fuel surrogate and their chemical mechanisms. In order to reproduce real fuels as well as possible, surrogates are required to closely emulate the thermo-physical properties and combustion characteristics of target jet fuels. Violi et al. [7] developed a JP-8 surrogate that contained six hydrocarbons and could emulate the distillation curve and thermo-physical properties of the target fuel. A detailed chemical mechanism of the surrogate was also presented in their work and validated by experimental data. Vasu et al. [8] evaluated the aforementioned chemical mechanism by comparing the measured and simulated IDT in a shock tube, and they reported that the mechanism could provide accurate IDT predictions above a temperature of 1000 K while predicting IDT poorly at low temperatures. Dagaut et al. [9] compared the kinetic modelling results of four jet fuel surrogates (one- and three-component mixtures of n-decane, n-propylbenzene, and n-propylcyclohexane) with JSR experimental data. The comparison results showed that the three-component surrogate was the most reliable substitute for the target fuel among all the test fuel surrogates. Gokulakrishnan et al. [10] developed a detailed kinetic model for the four-component kerosene fuel surrogate (n-decane/n-propylcyclohexane/n-propylbenzene/decene), which exhibited good performance in predicting the measured species concentrations. However, the IDT validations were not comprehensively conducted by them. Eddings et al. [11] proposed two six-component jet fuel surrogates named Hex-11 and Hex-12 to emulate a Jet-8 pool fire. The comparison results indicated that the surrogates could accurately capture the burning rate, emissive power, flame height, and puffing frequency of the steady-state pool fire. Dooley et al. [12] formulated a three-component jet fuel surrogate, 'MURI1' (n-decane/iso-octane/toluene), based on chemical group theory. The CN and H/C of the target fuel were regarded as the target properties of MURI1. Several devices, including a flow reactor and shock tube, were employed to validate the combustion properties of the proposed surrogate. They further developed an improved jet fuel surrogate named MURI2 comprising n-dodecane, iso-octane, n-propylbenzene, and 1,3,5-trimethylbenzene [13]. Apart from CN and H/C, TSI and MW were also selected as the emulating metrics. According to the ignition characteristic study conducted by Malewicki et al. [14], MURI2 exhibited a satisfactory performance on predicting the species profiles of small molecules including oxygen, carbon monoxide, carbon dioxide, and C1-C3 hydrocarbons. Kim et al. [15] proposed two four-component aviation fuel surrogates named UM1 and UM2 based on a model-based optimizer. The physical and chemical properties of the target fuel were reproduced by the two surrogates to some extent.

Despite the extensive research efforts directed towards the creation of various jet fuel surrogates and their accompanying kinetic mechanisms, notable limitations remain apparent in this scientific domain: (1) A recurring challenge is the inability of these surrogates to comprehensively replicate the intricate amalgamation of the physical and chemical properties characteristic of the target fuel. Achieving a harmonious equilibrium between these multifaceted attributes remains an elusive goal. (2) Furthermore, the chemical kinetic mechanisms developed for these surrogates have often exhibited tendencies towards impracticality. They tend to be excessively voluminous or overly intricate, thus impeding their direct application within the confines of practical engine combustion simulations. (3) In addition, the validation of these proposed surrogate mechanisms has not been exhaustive, especially when it comes to crucial parameters such as ignition delay time (IDT), species mole fractions, and flame speeds. The inadequacy of rigorous validation procedures raises pertinent concerns about the reliability and robustness of these surrogates in real-world applications. Addressing these limitations represents an imperative for the advancement of this field.

With the aim of addressing the mentioned issues, a four-component fuel surrogate incorporating the physical and chemical properties of real jet fuel was developed using a property optimizer. Eight properties, including CN, TSI, MW, LHV, H/C, liquid density, viscosity, and surface tension, were selected as the target physical and chemical properties. A reduced kinetic mechanism, comprising 124 species and 590 reactions, for the surrogate

was created which can prove advantageous in practical engine combustion simulations. Massive amounts of experimental data, including IDT, species concentration, and laminar flame speed, were collected to validate the mechanism from two aspects: the surrogate mixture and its components.

2. Formulation of Jet Fuel Surrogate

2.1. Target Fuel and Its Properties

The fuel combustion process inside an engine is very complex and always involves intricate physical and chemical processes. As shown in Figure 1, the fuel jet is injected into the cylinder via an injector, breaks down to small liquid droplets under the action of air shear force, and then evaporates and mixes with air to form a combustible fuel–air mixture. The processes are heavily affected by fuel physical properties such as viscosity, liquid density, and surface tension [16,17]. After that, the spontaneous ignition and combustion processes of the mixed fuel/air occur, where the chemical properties of the fuel have a significant influence on the events. Herein, CN dominates fuel ignitability, and MW plays a critical role in the diffusive transport process between liquid and the vaporized fuel. H/C influences the local ratio of fuel/air and adiabatic flame temperature, while LHV represents the energy generated from the fuel oxidation. Considering the above processes, eight properties, including CN, TSI, MW, LHV, H/C, liquid density, viscosity, and surface tension, were chosen as target properties for the surrogate in order to comprehensively reproduce the chemical and physical characteristics of real fuel in engine.

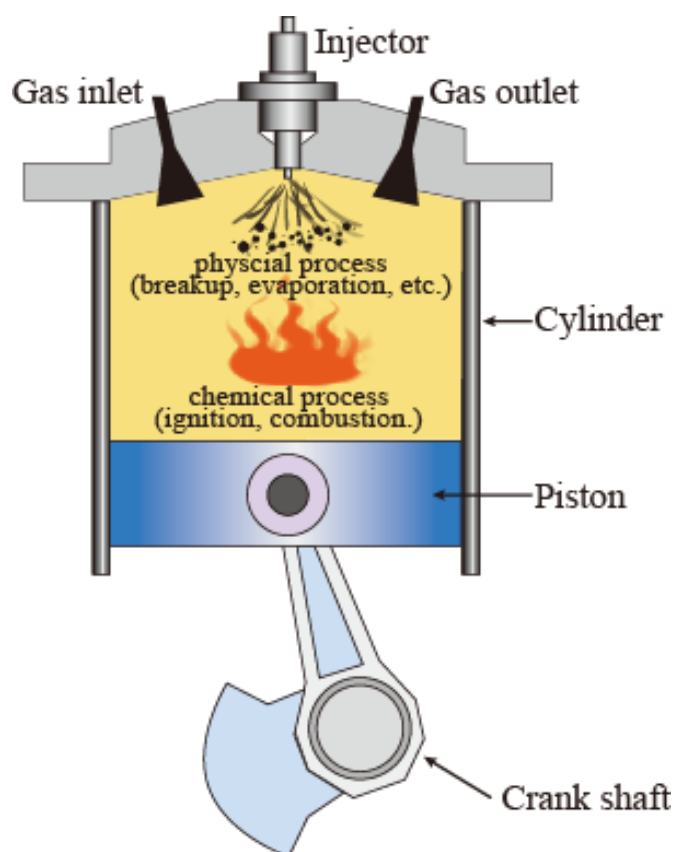


Figure 1. The physical and chemical processes in compression ignition engine.

In this work, Jet-A POSF-4658 (supplied by Edwards, AFRL-WP, Wright, OH, USA) was selected as the target real fuel for two reasons: First, it is a representative jet fuel comprising different jet-A batches, and its components and various properties have been extensively studied. Second, the experimental data on the IDT, laminar flame speed, and species concentration profiles of the fuel are available in the literature, so comparisons can be more readily conducted. However, since the data for LHV and surface tension of POSF-4658 are not available, the LHV of JP-8 fuel and surface tension of Jet-A were used instead as references in this study, similar to the previous studies [15,18]. The relevant properties of POSF-4658 were listed in Table 1.

Table 1. The properties of the target jet fuel [18].

Target Properties	Jet-A (POSF-4658)
CN *	47.1
MW	142 kg/kmol
H/C	1.957
LHV	43.23 MJ/kg
TSI	21.4
Liquid density	Temperature-dependent (See Figure 2)
Viscosity	Temperature-dependent (See Figure 2)
Surface tension	Temperature-dependent (See Figure 2)

* Derived cetane number (DCN).

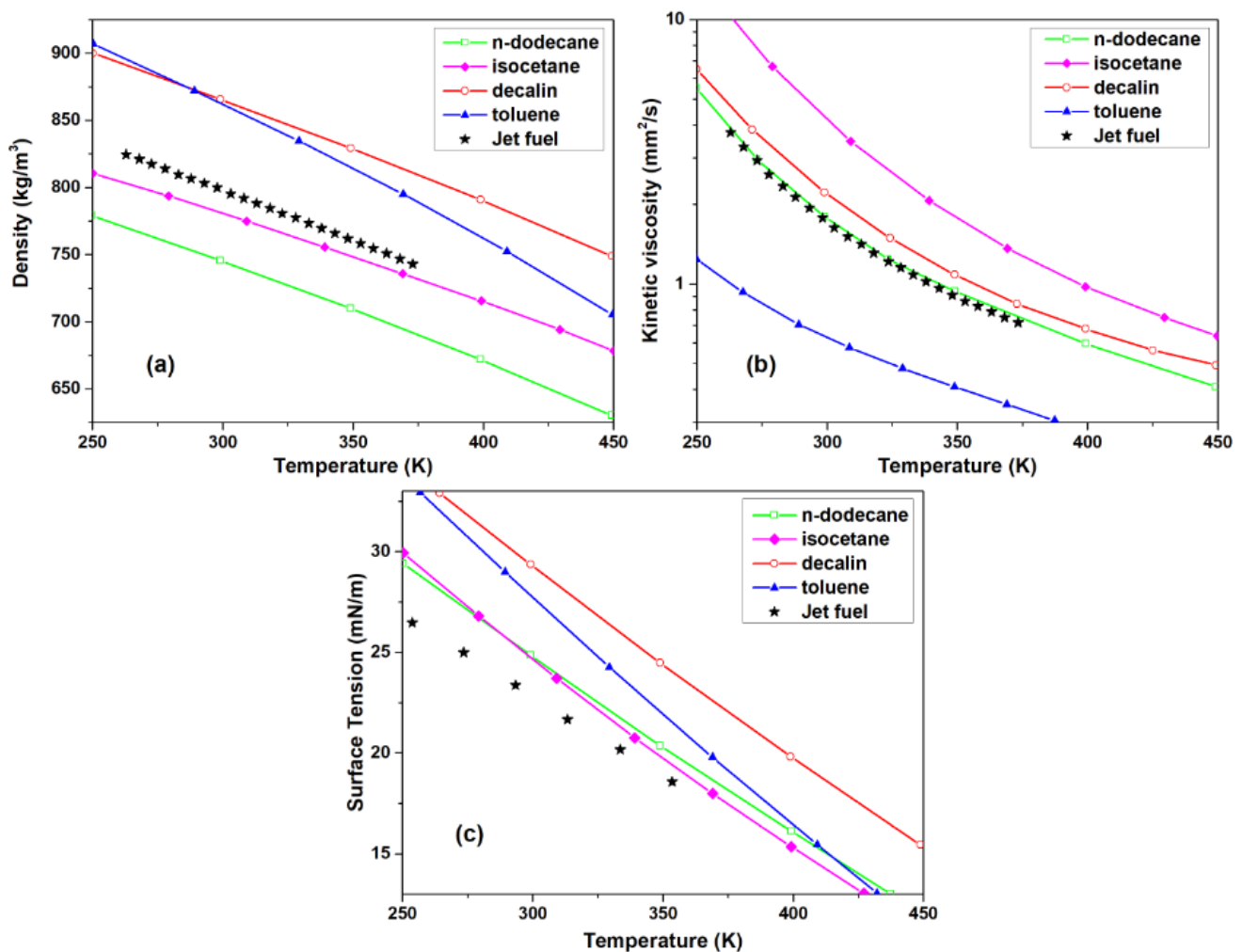


Figure 2. The temperature-dependent properties of the components: (a) density, (b) kinematic viscosity, and (c) surface tension.

2.2. Surrogate Fuel Components

Although real jet fuels contain a large number of compounds, according to Ref. [19], conventional jet fuels normally comprise 60% chain paraffins, 20% cycloalkanes, and 20% aromatics. Hence, it is reasonable to adopt the well-characterized compounds recognized in real jet fuels as the main surrogate components. Moreover, the components of jet fuel mainly belonged to C9–C16 hydrocarbons, which indicates that HC class and molecule size are also important criteria for surrogate components. The components whose chemical kinetic mechanisms have been well established are more preferred in our study. Based on these considerations, four components, including n-dodecane, isocetane, decalin, and toluene, were finally selected. The properties (CN, TSI, MW, LHV, and H/C) and formulae of the four components are listed in Table 2. The temperature-dependent properties, density, viscosity, and surface tension, are plotted in Figure 2. It can be easily seen that a single component is unable to represent real jet fuel because of the significant property differences between the single component and real fuel.

Table 2. The properties of the surrogate components.

Hydrocarbon Class Name	N-Alkane n-Dodecane	Iso-Alkane Isocetane	Cycloalkane Decalin	Aromatic Toluene
Formula	C ₁₂ H ₂₆	C ₁₆ H ₃₄	C ₁₀ H ₁₈	C ₇ H ₈
CN [20]	82.5	15	46.5	7.4
MW (g/mol)	170.33	226.44	138.25	92.14
LHV [21] (MJ/kg)	44.11	44.85	42.58	40.53
TSI [22]	7.0	22	22	40
H/C	2.17	2.13	1.8	1.1

2.3. Formation of Jet Fuel Surrogate

In this work, we improved the optimization algorithm from our previous study [18] to obtain the optimum component proportions of a jet fuel surrogate. The calculations for the target properties are showed in Table 3.

As reported in [20], the CN of the mixture can be calculated using the volume fraction average of the component CNs. The TSI of a mixture is obtained by calculating the mole fraction average of the pure component's TSI [23], while the LHV is estimated using the mass fraction average of the LHV. H/C and MW were directly determined by the component formula. The mixture density is also computed by the volume fraction average of component density. The viscosity is obtained using the Grunberg–Nissan equation [24,25], whereas surface tension is derived from the parachor correlation [26]. Finally, the equations proposed by Kim et al. [15] were employed as the merit functions:

$$\text{MeritFunc} = \sum_{i=1}^{\text{Num}_{\text{target}}} V_i \quad (1)$$

$$V_i = \frac{\sum_{j=1}^{\text{Num}_{\text{data},i}} \left(\frac{Q_{i,j,\text{cal}} - Q_{i,j,\text{exp}}}{Q_{i,j,\text{exp}}} \right)^2}{\text{Num}_{\text{data},i}} \quad (2)$$

where i and j represent the numbers of properties and experimental data points, respectively. $\text{Num}_{\text{data},i}$ refers to the total number of measurements of the i th property, and $\text{Num}_{\text{target}}$ represents the total number of target properties. $Q_{i,j,\text{cal}}$ and $Q_{i,j,\text{exp}}$ are the computed and measured properties, respectively.

Table 3. The estimation methods [18] of the properties of fuel surrogate.

Properties	Estimation Approaches
MW	Average of mole fraction: $\sum MW_{mix} = \sum X_i MW_i$ X_i is mole fraction of component i ,
H/C	$\frac{H}{C_{mix}} = \sum X_i \frac{H_i}{\sum X_i} C_i$ C_i is the number of carbon atoms of component i
TSI	Average of mole fraction: $TSI_{mix} = \sum X_i TSI_i$
LHV	Average of mass fraction: $LHV_{mix} = \sum Y_i LHV_i$
CN	Average of volume fraction: $CN_{mix} = \sum V_i CN_i$ V_i is volume fraction of component i
Density	Average of volume fraction: $\rho(T)_{mix} = \sum V(T)_i \rho(T)_i$
MW	Average of mole fraction: $\sum MW_{mix} = \sum X_i MW_i$
H/C	$\frac{H}{C_{mix}} = \sum X_i \frac{H_i}{\sum X_i} C_i$ H_i is the number of hydrogen atoms of component i ;
Viscosity	Grunberg–Nissan equation [24]: $\ln(\mu(T)_{mix}) = \sum X_i \ln(\mu(T)_i) + 0.5 \sum \sum X_i X_j G_{ij}$ G_{ij} is the binary interaction parameter
Surface tension	Parachor correlation: $\sigma(T)_{mix} = (P_{L,mix} \rho(T)_{L,mix,molar})^4$ $P_{L,mix} = 0.5 \sum \sum X_i X_j (P_i + P_j)$ $\sigma(T)_{mix}$ is liquid surface tension, P is parachor, $\rho(T)_{L,mix,molar}$ is liquid mixture molar density

A flowchart of the whole optimization process is given in Figure 3. It should be noted that the component will be removed when its mole fraction is less than 0.3% during the optimization process, the same as in our previous study [18]. Based on the above calculations, the optimum jet fuel surrogate was achieved, and it comprised 39.05% n-dodecane, 21.79% isocetane, 11.49% decalin, and 27.67% toluene by mole fraction and was abbreviated as JFS.

Table 4 shows the comparison results among the JFS surrogate and other jet fuel surrogates, including UM1, UM2, MURI2, S5 [27], and HEX12 [11]. In general, the property deviations of the surrogate JFS are less than 2% except for MW (10.73%), viscosity (5.88%), and surface tension (8.71%). The high deviations of MW and surface tension can be regarded as acceptable compared to other surrogates. As shown in Table 4, the deviation of the MW of S5 is 12.11%, and the averaged deviations of surface tension of UM2, Hex12, and S5 are larger than 15%, which are all larger than the corresponding property deviations of the surrogate JFS. It is also observed that the CN, MW, H/C and, LHV of the surrogate UM1 show good agreement with the target fuel; however, the deviations of TSI (−21.52%) and viscosity (−21.2%) are too large. The surface tension of UM2 deviates from the target property by 15.8%, even though CN, LHV, and density are well captured by the surrogate UM2. The LHV, MW, CN, and H/C are well emulated by MURI2; however, the deviation of viscosity (34.608%) is too large. As for the properties of HEX12 and S5, the majority of them greatly deviate from the target properties. Overall, the surrogate JFS performs better than other surrogates at reproducing the chemical and physical properties of real jet fuel; hence, it is more likely to be adopted for practical engine combustion simulation.

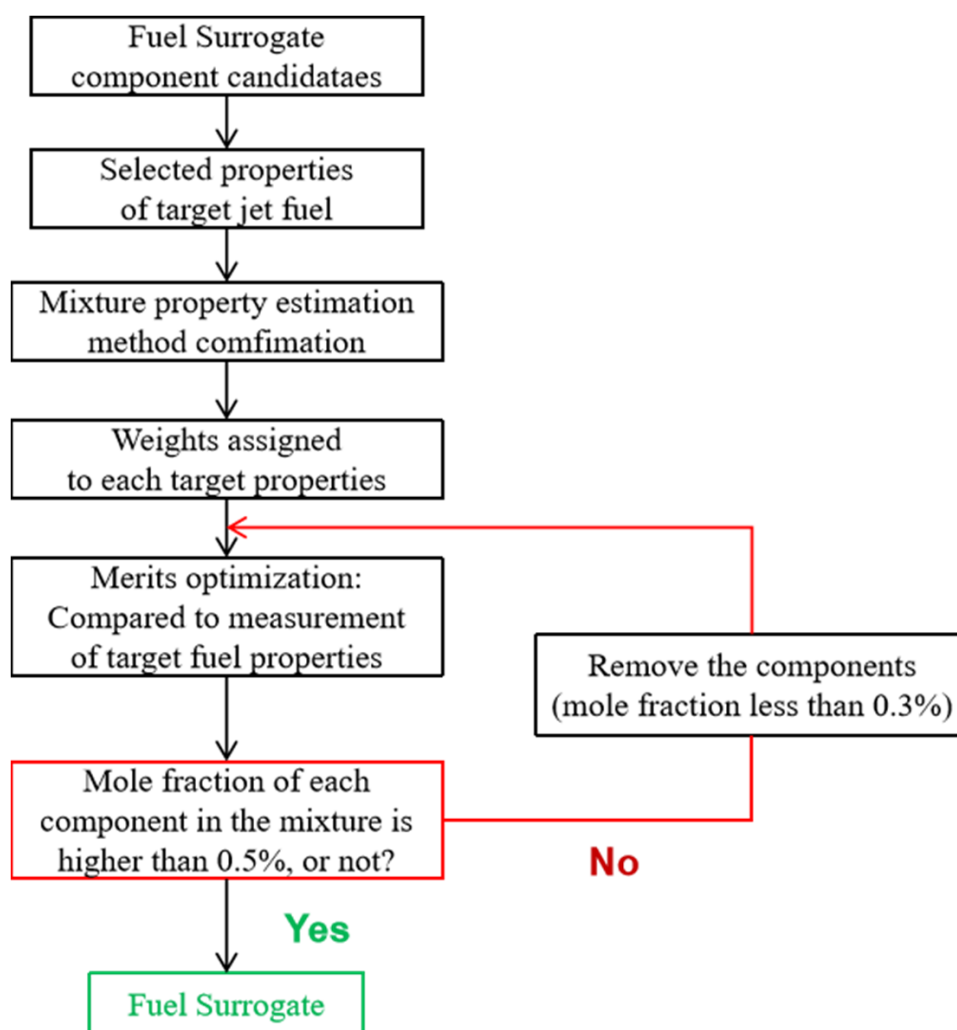


Figure 3. The flow chart of optimization process for the jet fuel surrogate.

Table 4. The comparison results among JFS and other jet fuel surrogates.

Jet Fuel	Surrogate	JFS	UM1	UM2	MURI2	S5	HEX12
CN 47.1	Val	46.93	46.8	46.7	48.5	32.1	60.5
	Dev (%)	−0.35	−0.64	−0.85	2.97	−31.8	28.45
H/C 1.957	Val	1.94	1.967	1.881	1.950	1.807	1.856
	Dev (%)	−0.86	0.51	−3.88	−0.36	−7.66	−5.16
MW 142	Val	157.23	143.5	148.6	138.7	159.2	152.2
	Dev (%)	10.73	1.06	4.65	2.32	12.11	7.18
LHV	Val	43.61	43.62	43.36	43.55	43.02	44.6
	Dev (%)	0.87	0.90	0.30	0.74	−0.49	3.17
TSI 21.4	Val	21.12	16.79	22.14	20.4	34.61	25.0
	Dev (%)	−1.29	−21.52	3.45	−4.67	61.72	16.84
Density	Average dev (%)	1.84	−3.4	0.6	−5.518	2.392	1.423
Viscosity	Average dev (%)	5.88	−21.2	−3.6	−34.608	18.167	5.077
Surface tension	Average dev (%)	8.71	9.1	15.8	3.131	19.1	18.774

3. Kinetic Modelling

3.1. Methodology

In this study, to facilitate the simulation of a practical engine combustion, a so-called decoupling methodology [5,18] was adopted for developing the JFS chemical mechanisms. The chemical kinetic mechanism was established through a systematic formation process, starting from C16 reactions and progressing towards H₂/O₂/C1 reactions. The subsequent steps involved incorporating a NO_x sub-mechanism and polycyclic aromatic hydrocarbon (PAH). The reduction and optimization procedures employed in this process are briefly outlined as follows:

- (1) The initial stage of the reduction and optimization process involves conducting a reaction pathway analysis to identify the key reactions. Subsequently, unimportant species and reactions are eliminated from the initial kinetic model. Simultaneously, the rate of production (ROP) and sensitivity analyses are performed to evaluate the remaining species and reactions. This allows for a clear understanding of the impact of each reaction on the oxidation process.
- (2) Subsequently, the reaction rate constants were optimized to improve the agreement between the simulated and experimental data of fuel ignition delay time (IDT).
- (3) Afterward, the concentrations of species and laminar flame speeds predicted by the reduced mechanism were compared to the corresponding measurements. This allowed for references to fine-tune the reaction rate constants further.
- (4) Steps 1 to 3 were iteratively repeated until the desired size and accuracy of the mechanism were attained.

3.2. Toluene Sub-Mechanism

The current chemical kinetic model mainly comprises four sub-mechanisms, including the toluene sub-mechanism, decalin sub-mechanism, n-dodecane sub-mechanism, and isocetane sub-mechanism (Figure 4).

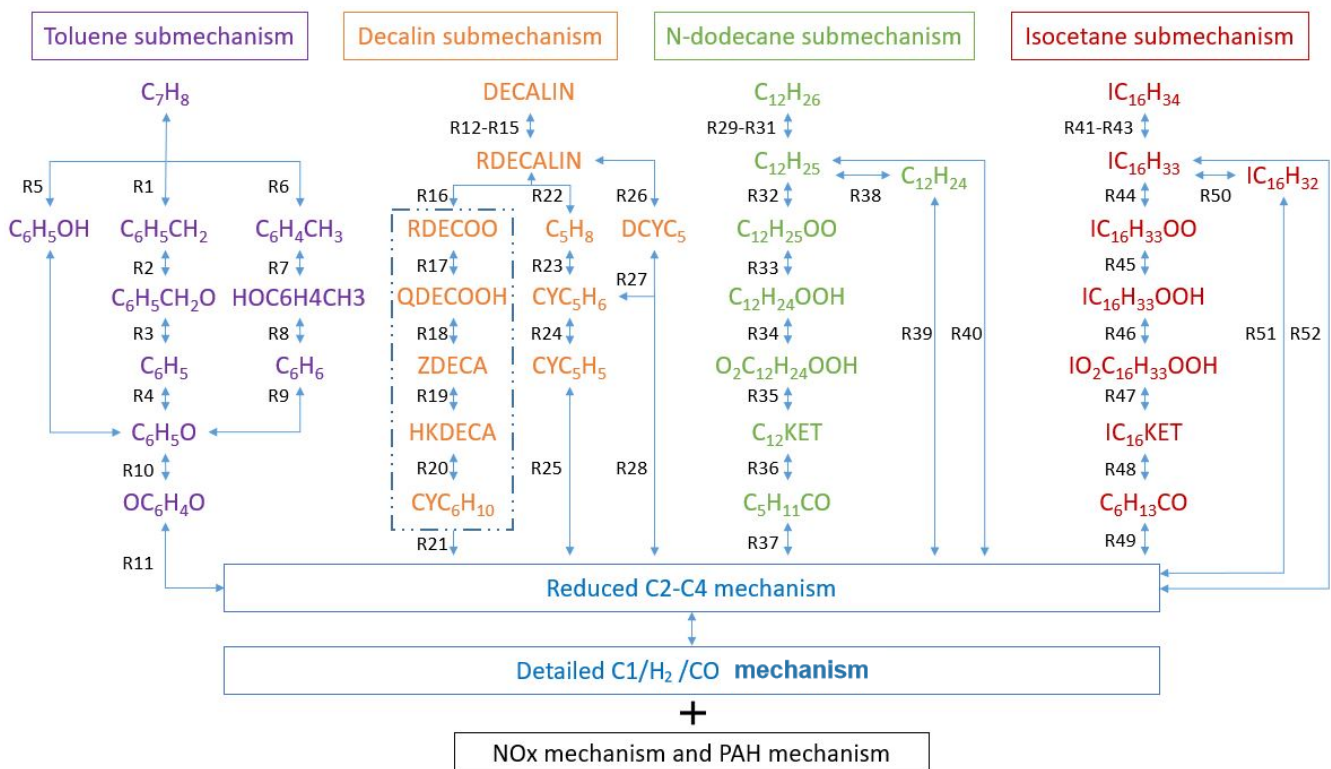


Figure 4. The major reaction pathways for the JFS kinetic mechanism.

The toluene sub-mechanism was tuned from the reduced TRF-PAH mechanism [28], and it was employed as the initial mechanism based on two reasons: (1) The size of the TRF-PAH mechanism is compact, which is advantageous for three-dimensional engine combustion simulation; and (2) The mechanism has good performance in predicting species concentrations and flame speeds.

Figure 4 illustrates the principal reactions of the reduced toluene mechanism. Toluene is predominantly consumed through three pathways: the H-atom abstraction reactions leading to the production of $C_6H_4CH_3$ (R6), $C_6H_5CH_2$ (R1), and the reaction R5. Among these, the formation of $C_6H_5CH_2$ is the primary pathway for toluene consumption, while C_6H_5OH ranks as the second most abundant product. Through some intermediate species, such as $C_6H_5CH_2O$, C_6H_5 , and C_6H_5O , the toluene molecule ultimately converts into the small molecules. Some species, such as $C_6H_5CH_2OO$, C_6H_5CO , and $OC_6H_4CH_3$, which are absent in Figure 4, were also incorporated into the toluene sub-mechanism.

The NO_x and PAH sub-mechanisms of the original TRF-PAH mechanism were retained in the current mechanism. The NO_x sub-mechanism includes four species and 12 reactions, and it contains thermal reactions and N₂O-intermediate reactions. The PAH mechanism is able to reproduce PAH formation up to a four-ring PAH. Herein, H-atom abstraction reactions, methyl substitution reactions, and hydrogen abstraction acetylene addition (HACA) make great contributions to PAH formation, and hence the reactions of MAHs (e.g., A_1C_2H and $A_1C_2H_3$) were considered. As reported in Ref. [28], the predictions obtained from the PAH mechanism demonstrated outstanding agreement with the measured data collected from eight different flames, which indicated that the present PAH mechanism is satisfactory to some extent.

3.3. Decalin Sub-Mechanism

The decalin mechanism was reduced from the detailed decalin oxidation mechanism proposed by Dagaut et al. [29]. As shown in Figure 4, the current decalin mechanism contains both low- and high-temperature mechanisms, and so the mechanism exhibits the capability to accurately describe decalin oxidation across a broad temperature range. The reactions framed by the dashed box (Figure 4) belong to the low-temperature mechanism.

Decalin radicals can be diverse considering the symmetrical structure of a decalin molecule. Three $C_{10}H_{17}$ radicals lumped as 'RDECALIN' were produced via decalin consumption reactions with small molecules including O_2 , H, and HO_2 , as shown in Figure 4 (R12–R15). In accordance with Yu et al. [30], the low-temperature and high-temperature mechanisms exhibit significant differences in their core reactions. In the low-temperature regime, the primary consumption pathway for RDECALIN involves the O_2 addition reaction (R16), while other consumption reactions are negligible. The formation of alkylperoxy radicals (RDECOO) via R16 is followed by their isomerization to hydroperoxy alkyl (QDECOOH). QDECOOH, in turn, undergoes a conversion to ZDECA (lumped $C_{10}H_{17}O_4$ isomers) through the reaction R18. ZDECA is then consumed, leading to the formation of $C_{10}H_{16}O_3$ isomers (KHDECA), and the decalin chain-branching sequence is completed by the reaction R20, which represents the KHDECA decomposition at low temperatures. Conversely, in the high-temperature regime, the decomposition of RDECALIN primarily occurs through reactions that tend to generate C_5H_8 species and cyclopentyl-cyclopentene (DCYC5). Then C_5H_8 decomposes to cyclopentadiene (CYC_5H_6) via the H-abstraction reaction (R23). Eventually, the big hydrocarbon molecules are converted into small C2–C4 molecules.

3.4. N-Dodecane Sub-Mechanism

The n-dodecane mechanism was reduced via our previous work [31] and was briefly introduced here. As shown in Figure 4, n-dodecane is consumed by three reactions (R29–R31) to produce dodecyl radicals ($C_{12}H_{25}$) at low temperatures. $C_{12}H_{25}$ then transforms to peroxy dodecyl radicals ($C_{12}H_{25}OO$) via the pathway reaction R32, which is significant for the formation of the negative temperature coefficient (NTC) region. Hydroperoxy dodecyl

radicals ($C_{12}H_{24}OOH$) are produced by a isomerization reaction (R33). $C_{12}H_{24}OOH$ transforms into $O_2C_{12}H_{24}OOH$ by reacting with oxygen (R34). $C_{12}KET$ radicals are produced from the reaction R35, and they further decompose into a few species, including $C_5H_{11}CO$, with the reaction R36. The small species will be generated through the decomposition reaction R37. However, at high temperatures, dodecyl radicals first convert to $C_{12}H_{24}$ by a reaction with oxygen (R38) and then decompose into C2–C4 molecules via the reaction R39 or directly produce the small hydrocarbon molecules by R40.

3.5. Isocetane Sub-Mechanism

The isocetane sub-mechanism was also taken from our previous work [32]. A short depiction of the isocetane sub-mechanism is given here. The consumption of isocetane is completed by the reactions R41–R43 at low temperatures (Figure 4). Ketohydroperoxide is produced via the reactions R44–R47, while the decomposition of ketohydroperoxide is completed by the reactions R48 and R49. At high temperatures, all reactions are represented by the three reactions R50, R51, and R52.

4. Results and Discussion

The experimental data, including IDTs, species concentrations, and laminar flame speeds determined by various devices, were used for validating the current kinetic mechanism. The mechanism was first validated for each component and then for the surrogate fuel mixture. The validation of the individual components will give a more comprehensive assessment on the accuracy and reliability of the JFS mechanism. The simulations were performed on CHEMKIN-PRO Version-19.0 software [33].

4.1. Verifications of Toluene

4.1.1. IDT

It is necessary to validate the current mechanism on IDT because the fuel autoignition behaviors characterized by IDT are important for engine combustion and emission performances [34]. Figure 5 exhibits a comparison of the measured and simulated IDTs for toluene in a shock tube under varying conditions of temperature, pressure, and equivalence ratios. The measurements were determined by Shen et al. [35], and the predicted IDT with the current mechanism and the based mechanism [28] were exhibited. Both the reduced mechanism and the based mechanism demonstrated strong agreement with the measurements. The current mechanism showed better performance under an equivalence ratio of 1.0. Compared to the based mechanism, the IDTs predicted by the current mechanism are closer to the measurements at low pressure. In addition, the predicted IDTs of toluene are compared with the determined IDTs in an RCM [36]. The corresponding results are presented in Figure 6. The toluene IDTs were slightly underestimated, but the discrepancy is acceptable.

4.1.2. Species Concentration

As emphasized by Pitz et al. [37], it is equally crucial to validate the profiles of major species concentrations alongside the validation of fuel IDT. Hence, the current mechanism was validated for the major species profiles during the oxidation process. In Figure 7, the concentration profiles of critical species in the premixed toluene flame are displayed. These species include reactants (toluene and oxygen), an inactive gas (argon), and products (such as carbon monoxide and hydrogen). Li et al. [38] experimentally investigated premixed toluene flames at three equivalence ratios ($\Phi = 0.75, 1.0, \text{ and } 1.5$) under a pressure of 10 atm. A satisfactory agreement was observed between the predicted and observed species profiles for all flames, with a notable consistency observed in the case of the stoichiometric toluene flame. The argon species concentration initially decreased and then stabilized further downstream of the burner. The model accurately predicted this trend, demonstrating its capability to replicate the mole expansion effects observed in the toluene flame, as reported in reference [38]. Additionally, the model successfully captured

the overall profiles of the final products, specifically water and carbon dioxide, and the maximum deviations between the measurements and predictions for final products are less than 10%. Carbon monoxide displayed a profile resembling that of hydrogen, gradually surpassing carbon dioxide as the predominant carbon product. Despite the discrepancies in the predicted species concentrations of toluene and oxygen compared to the corresponding measurements at equivalence ratios of 0.75 and 1.5, the model successfully represented the depletion positions of these species with accuracy.

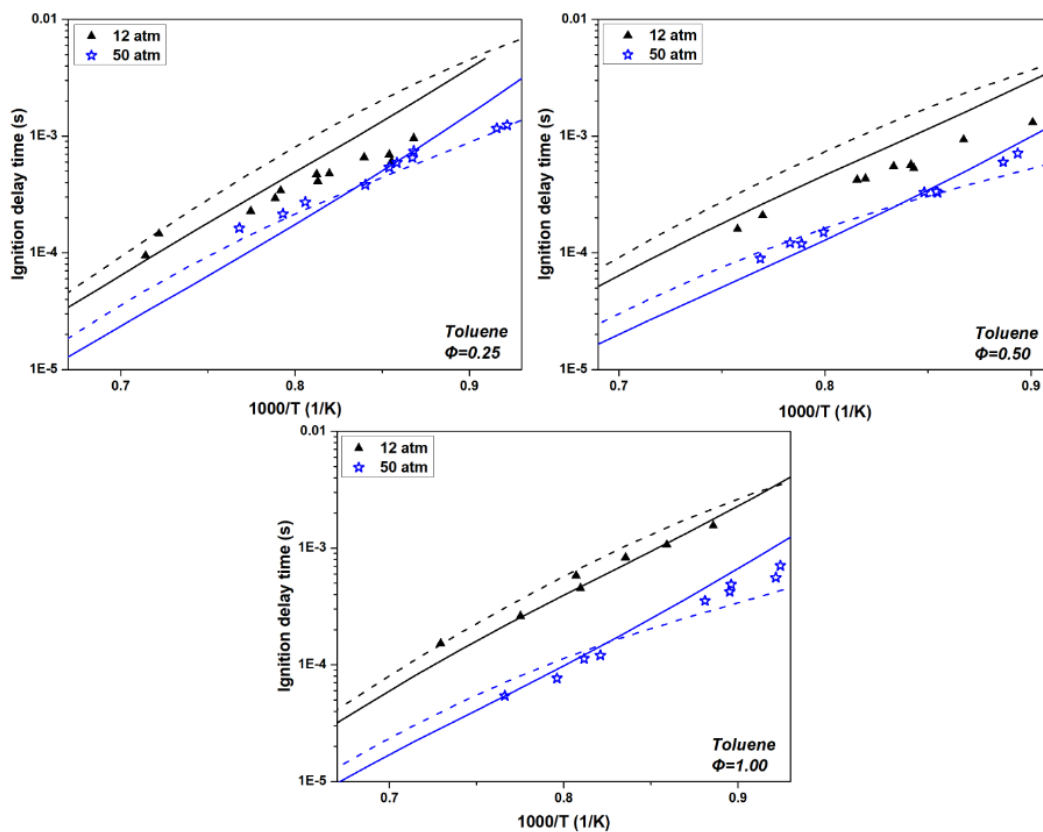


Figure 5. The measured (symbols [35]) and predicted (solid lines: current mechanism, dash lines: the based mechanism [28]) toluene IDTs determined in shock tube.

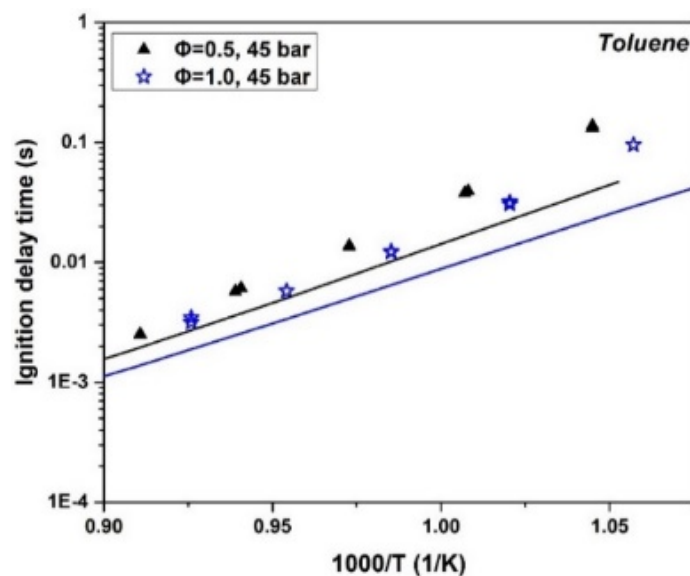


Figure 6. The measured (symbols) and simulated (lines) toluene IDTs in RCM.

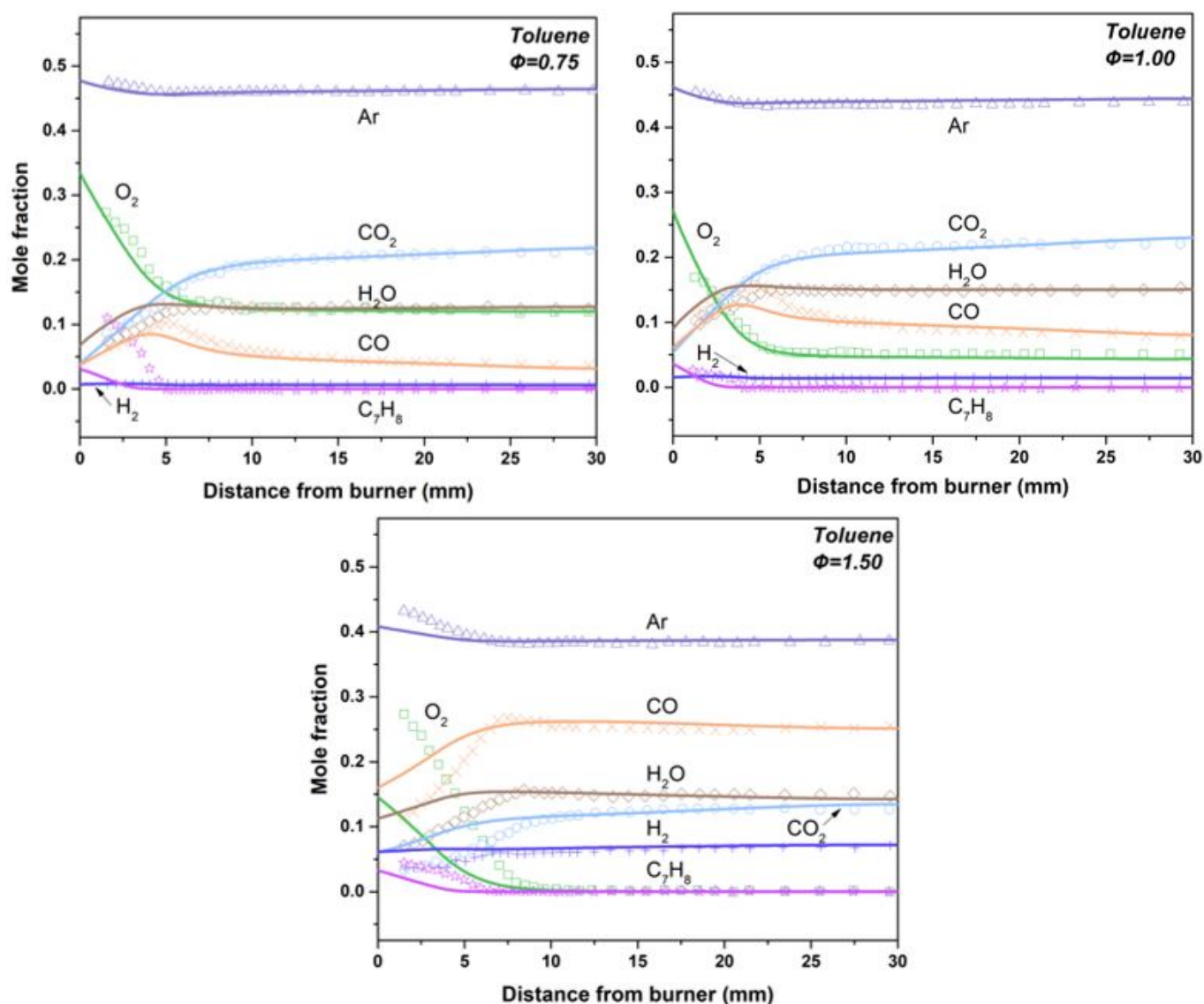


Figure 7. The major species profiles of premixed toluene flames under three equivalence ratios (0.75, 1.0, and 1.5) and a pressure of 10 atm. The determined results [38] are represented by symbols, while the simulated values from the current mechanism are depicted by lines.

Figure 8 shows the toluene oxidation process in a JSR [39] at a residence time of 0.6 s and a pressure of 10 atm. The concentration evolution of both the major species (CO , CO_2 , and C_7H_8) and the minor species (C_2H_2 and C_4H_4) are presented in Figure 8. The current mechanism rendered good performance in predicting the concentration profiles of C_7H_8 , CO , and CO_2 . C_2H_2 is esteemed as a significant precursor of PAH and soot formation [40]. Moreover, the proposed model exhibits its capability to predict the toluene concentration evolution. Furthermore, the mechanism successfully predicted the species profiles of C_4H_4 under different conditions, except for the scenario with an equivalence ratio of 1.5.

4.1.3. Laminar Flame Speed

The laminar flame speed (LFS) is a valuable parameter that provides insights into the reactivity, heat release rate, and propagation characteristics of actual fuels. Figure 9 shows the comparison between the simulated and measured LFSs of counter-flow toluene flames. The measurements were conducted under two conditions: $p = 1$ atm, $T_u = 298$ K [41], and $p = 3$ atm, $T_u = 450$ K [42], where T_u denotes the temperature of the unburned mixture. It can be observed that the mechanism performed well in predicting the flame

behavior under atmospheric conditions. However, the discrepancy of the predictions and measurements were larger under fuel-rich conditions compared to oxygen-rich conditions. Therefore, we can conclude that the current mechanism is more suitable for modeling lean-burn engine combustion.

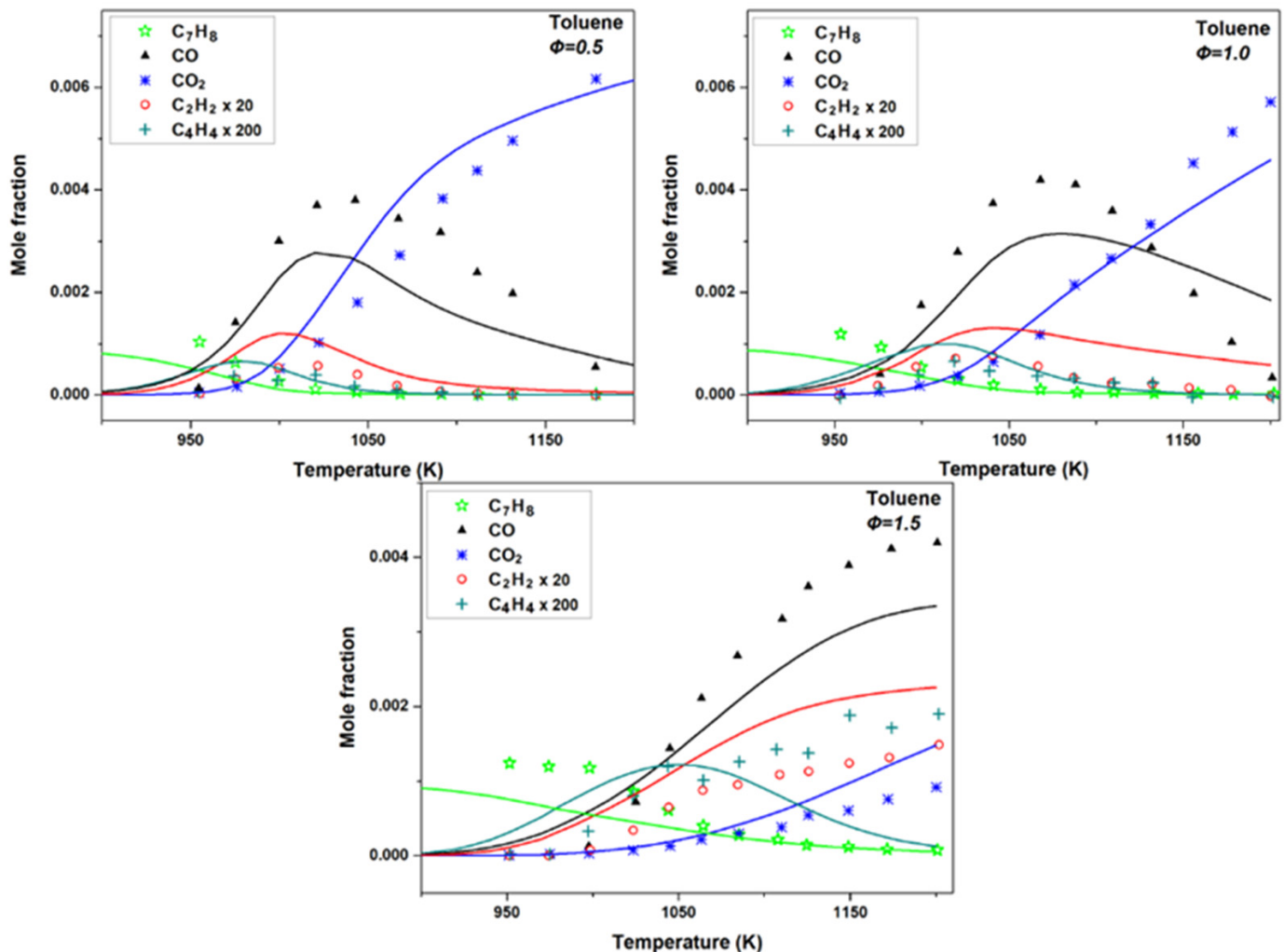


Figure 8. The concentrations of species resulting from the oxidation of toluene in the JSR are presented for various equivalence ratios at 0.6 s residence time and a pressure of 10 atm. The measured values [39] are denoted by symbols, while the simulation results obtained by the current mechanism are represented by lines.

4.2. Verifications of Decalin

4.2.1. IDT

Figure 10 displays the comparisons of the simulated and measured ignition delay times for decalin in a shock tube. The experimental data were obtained from previous studies [43,44], while the simulation results were obtained with both the present mechanism and the detailed mechanism [29]. Except for the case of $\Phi = 0.5$ and $p = 12$ atm, the current mechanism consistently outperformed the detailed mechanism across all other conditions, as demonstrated in Figure 10. However, considering the results achieved by the detailed mechanism, the level of discrepancy observed under the mentioned condition is still within an acceptable range. These results confirm that the current mechanism effectively captures the dependence of IDT on pressure and equivalence ratio, particularly at two specific conditions: (1) $p = 20$ atm, $\Phi = 0.5$; (2) $p = 40$ atm, $\Phi = 1.0$.

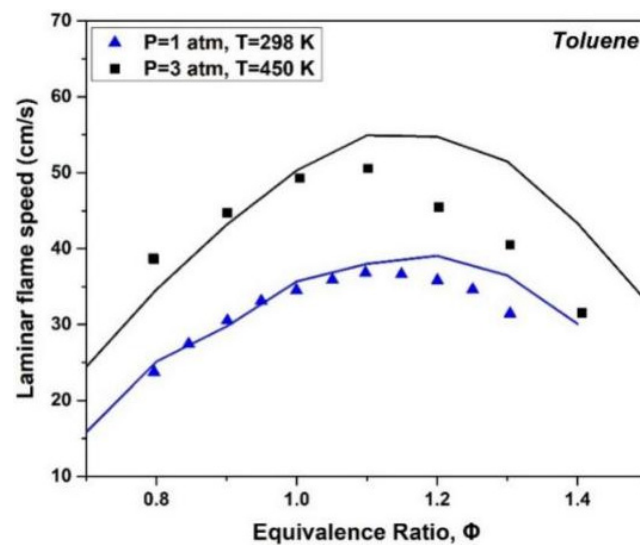


Figure 9. The simulated and measured LFSs in counter-flow toluene flames.

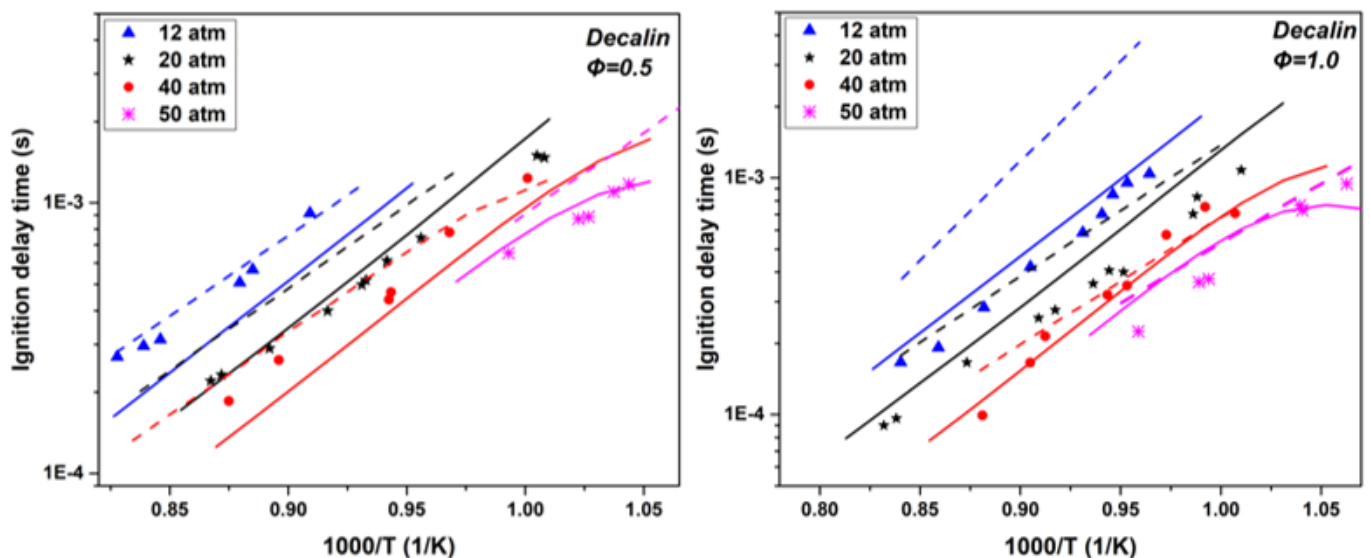


Figure 10. The measured (symbols) and predicted IDTs (solid lines: current mechanism; dash lines: the detailed mechanism) for decalin in a shock tube.

Figure 11 depicts the ignition delay time (IDT) of decalin over a temperature range of 770 K to 1250 K. Non-thermal combustion (NTC) behaviors were observed within this temperature range. At low-pressure conditions ($p = 20$ atm), the NTC region started at around 910 K, while at high temperatures, the NTC region initiated at a higher temperature of approximately 940 K. The shift in the NTC region suggests that pressure significantly influences the NTC behavior, which aligns with similar findings reported in Ref. [45].

In Figure 12, the decalin IDT is presented as determined in a rapid compression machine over a broad temperature range. The measurements were conducted at various equivalence ratios and a 15 atm compression pressure [30]. The results clearly demonstrate that IDTs decrease with increasing equivalence ratios. The variations in IDTs among different conditions were relatively small within the temperature range of 631 to 750 K, indicating a weak influence of equivalence ratio on IDTs at low temperatures. As the temperature increased, the differences in the ignition delay times (IDTs) became more pronounced. This can be attributed to the intensified chain-branch reactions occurring between the decalin molecules and hydroperoxyl radicals in both the negative-temperature-

coefficient and high-temperature zones. The current mechanism successfully captures these observed behaviors.

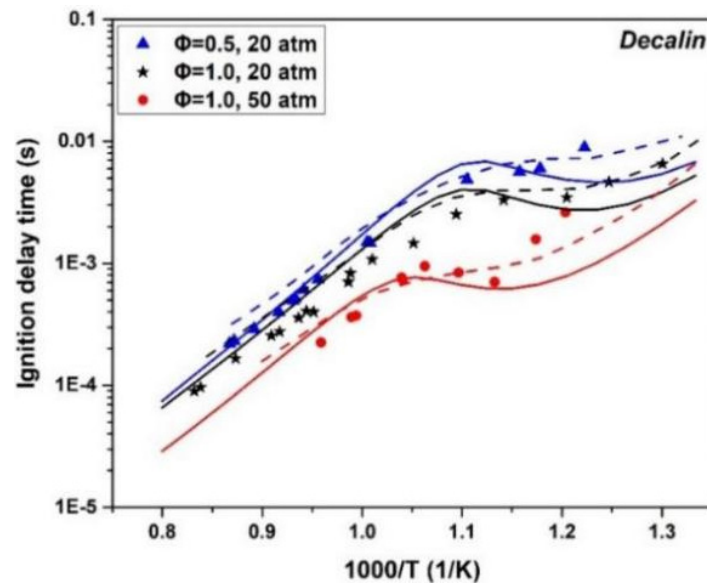


Figure 11. The decalin IDTs' NTC behaviors in a shock tube. The measured (symbols [43,44]) and predicted IDTs (solid lines: current mechanism; dash lines: the detailed mechanism [29]) for decalin.

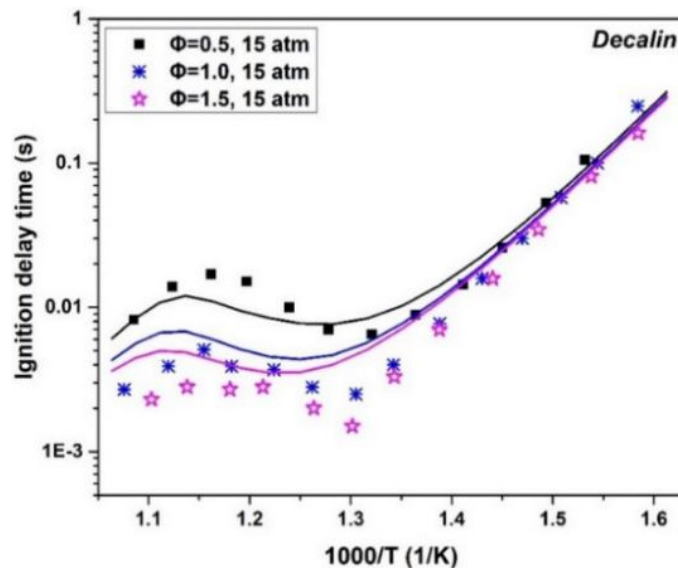


Figure 12. The measured (symbols) and predicted (lines) decalin IDTs in a RCM at three equivalence ratios under 15 atm compression pressure.

4.2.2. Species Concentration

Figure 13 exhibits the species profiles of the premixed decalin flames [46]. The predictions and measurements showed excellent agreement across various equivalence ratios. According to the ROP analysis, CO is predominantly generated through reactions involving HCO and HCCO, while its consumption occurs through its reaction with hydroxyl radicals, leading to the formation of CO₂. The formation of H₂O is notably influenced by H-atom abstraction reactions as well as the reaction between OH and H₂. H₂ is produced through a reaction between decalin and formaldehyde (CH₂O). The positions of depletion for decalin species varied with different equivalence ratios, and in the case of the stoichiometric decalin flame, the depletion position was observed to be closer to the burner surface. Similar observations were reported in the referenced study [38].

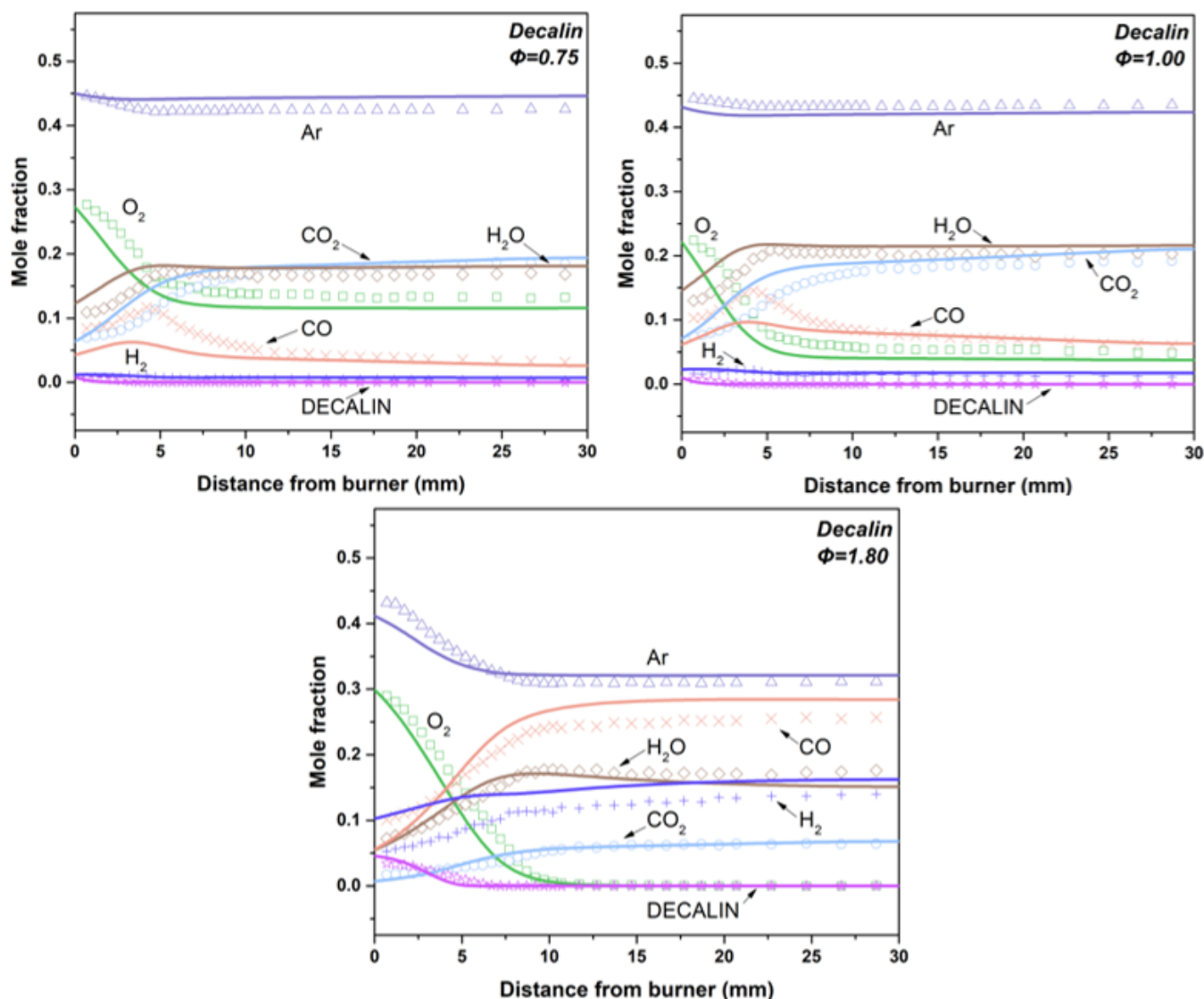


Figure 13. The premixed decalin flames species profiles at various equivalence ratios. The measured values [46] are denoted by symbols, while the simulated values from the current mechanism are represented by lines.

The species concentration profiles of decalin were also examined in the JSR [29]. C_2H_2 and CH_4 were selected for validating the accuracy of the current mechanism since they are the significant intermediate hydrocarbons produced during decalin oxidation. The current mechanism accurately predicted the concentration variations of C_2H_2 and CH_4 , although it slightly overestimated the decalin concentration. It was observed that the concentration of CO initially increased and then reached a steady level above 900 K. The concentration of CO_2 exhibited a continuous increase with rising temperature. Overall, the current mechanism demonstrated good performance in reproducing these trends. Furthermore, the concentration profiles of CH_2O , a major aldehyde produced during the oxidation process of decalin, were also accurately captured by the current mechanism (Figure 14).

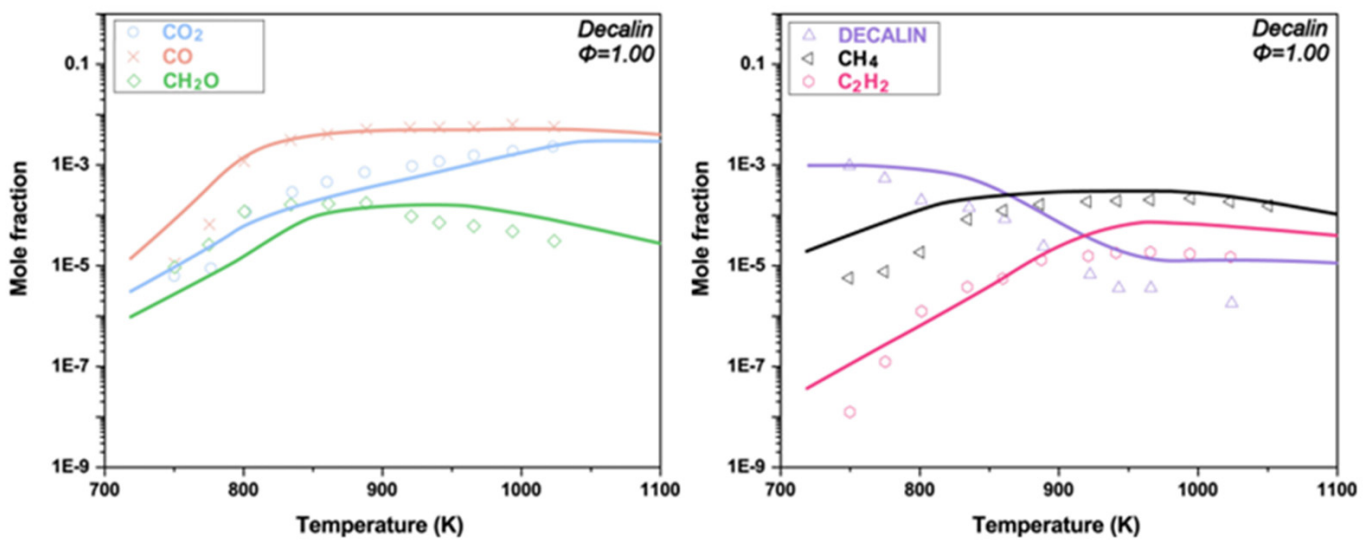


Figure 14. The measured (symbols [29]) and predicted (lines) concentration profiles of species resulting from the oxidation of decalin in the JSR at an equivalence ratio of 1.0 and a compression pressure of 10 atm.

4.2.3. Laminar Flame Speed

Figure 15 illustrates the determined and predicted LFSs for the counter-flow decalin flame at atmospheric pressure [47]. The initial mixture temperature for the flame is 443 K. It is evident that the current mechanism accurately predicts the laminar flame speed of decalin, although the deviation between measured and predicted LFSs becomes larger under high equivalence ratios.

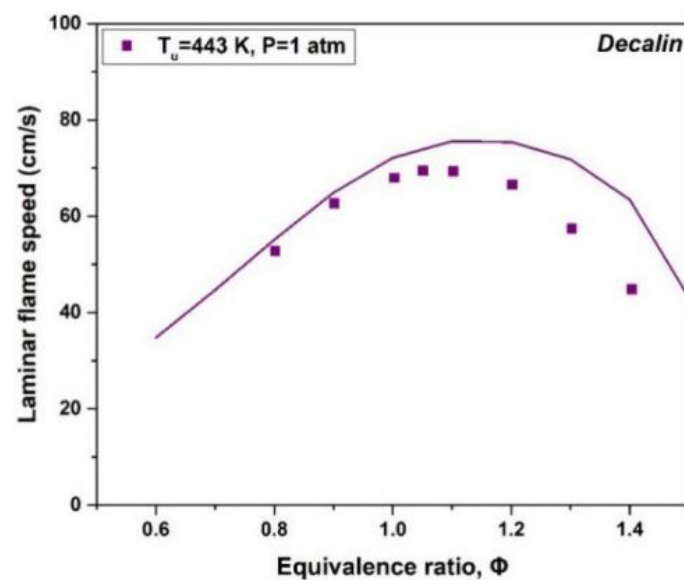


Figure 15. The laminar flame speeds of the counter-flow decalin flame. The line stands for the simulations, and dots represent the experimental data [47].

4.3. Verifications of *n*-Dodecane

4.3.1. IDT

Figure 16 shows the predicted and measured *n*-dodecane IDTs at two equivalence ratios (0.5 and 1.0) under three pressures (14 atm, 20 atm, and 40 atm). The shock tube measurements were taken from the Refs. [48–50]. The results confirmed that the current mechanism was capable of capturing the variation trends of the measured IDTs, except in

the case of $p = 40$ atm. The NTC behaviors observed in the temperature range from 750 K to 900 K were well reflected by the mechanism. In addition, the experimental phenomenon that IDT decreases with an increase in pressure was also captured by the mechanism.

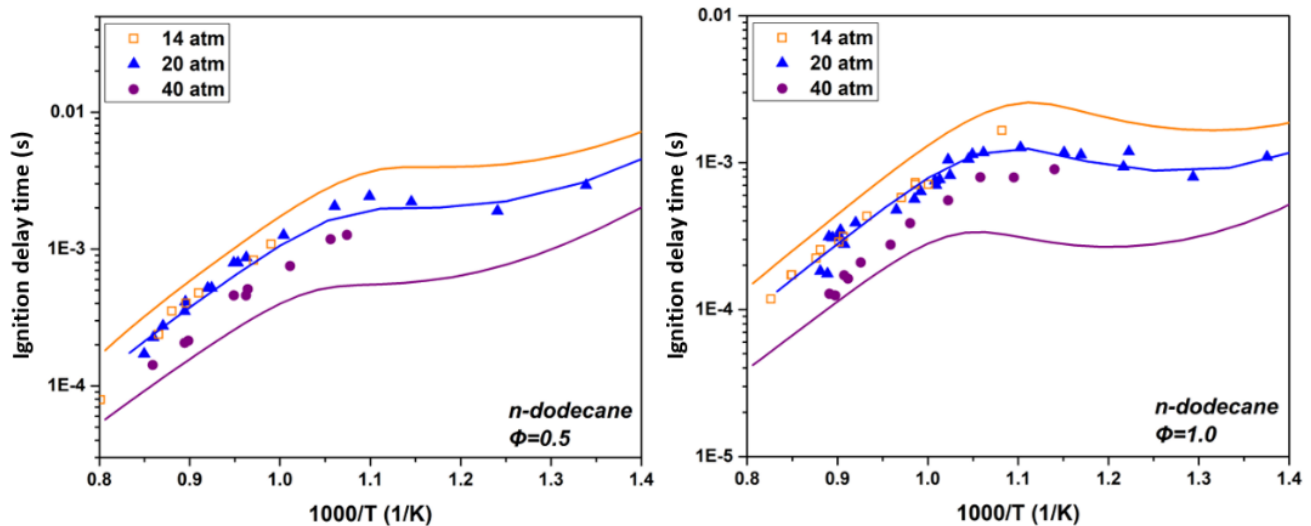


Figure 16. The measured (symbols) and predicted (lines) IDTs of n-dodecane in shock tube.

4.3.2. Species Concentration

Malewicki et al. [14] conducted JSR experiments to investigate the n-dodecane oxidation process. The experiments were carried out at a residence time of 1 s, a pressure of 10 atm, and three equivalence ratios. The comparison between the computed and measured results is shown in Figure 17. The prediction for the variation trend of O_2 and n-dodecane ($C_{12}H_{26}$) with temperature was consistent with the measurements under all conditions. H_2O was slightly underestimated, but the deviation is still at an acceptable level. There were some deviations between the simulated and determined mole fractions of C_2H_2 and CO_2 ; nevertheless, the overall simulated profiles of C_2H_2 and CO_2 were satisfactory.

4.3.3. Laminar Flame Speed

The measured data of the n-dodecane laminar flame speed were adopted here from the experiment conducted by Kumar et al. [51]. The measurement was performed at atmospheric pressure and unburned mixture temperatures of 400 K and 470 K. It can be easily seen from Figure 18 that the predictions showed fairly good agreement with the experimental data under all conditions.

4.4. Verifications of Isocetane

4.4.1. IDT

The IDTs of isocetane were measured in a shock tube under two pressures (10 atm and 40 atm) and three equivalence ratios (0.5, 1.0, and 1.5) by Oehlschaeger et al. [52]. Figure 19 presents the predictions and measurements of isocetane IDT, and the maximum deviations between the measured and predicted IDT appeared under the condition of $p = 10$ atm and $\Phi = 1.0$, confirming the derived mechanism can accurately predict IDT. The decreasing trend of IDT with increasing pressure was perfectly captured by the mechanism. Due to the absence of experimental data, the NTC behaviors were not obviously observed at low pressure and low equivalence ratios. Therefore, it is necessary to do further IDT validations for isocetane in the future.

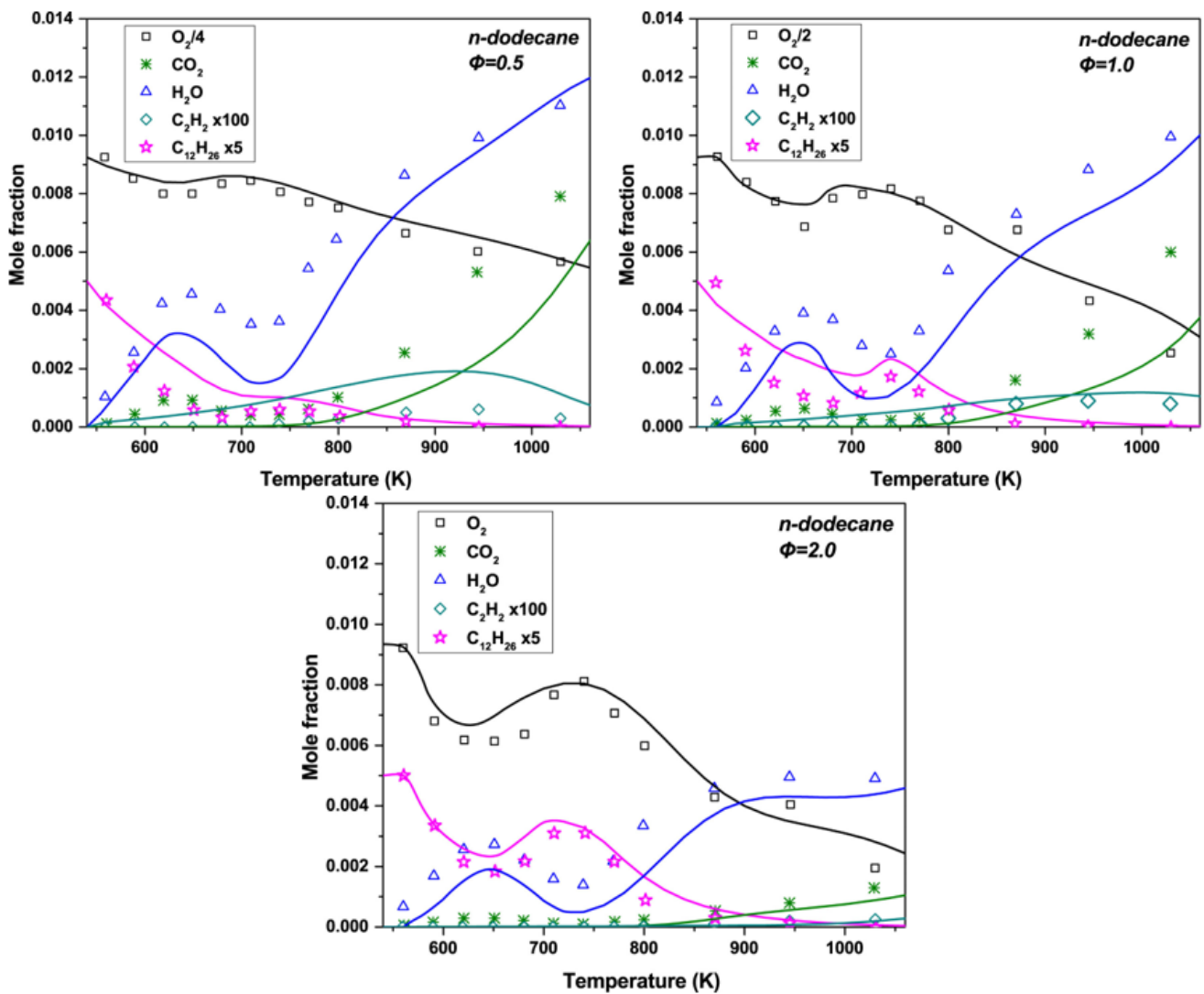


Figure 17. The measured (symbols [14]) and predicted (lines) mole fractions of the species during n-dodecane oxidation in JSR experiments at different equivalence ratios.

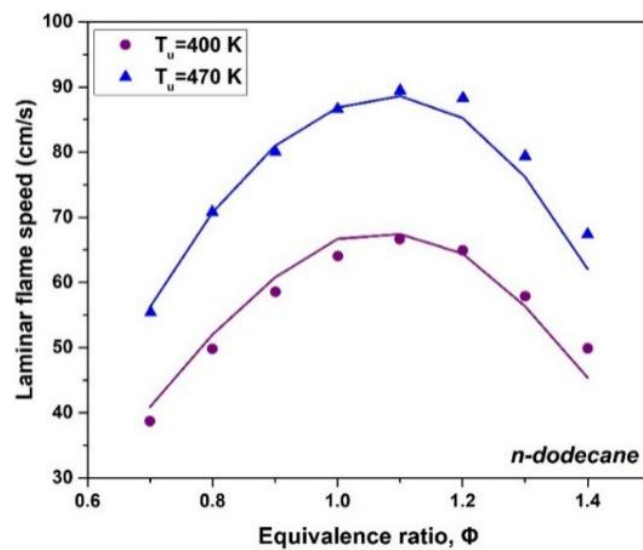


Figure 18. The laminar flame speeds of the n-dodecane flame. The line stands for the simulations, and dots represent the experimental data [51].

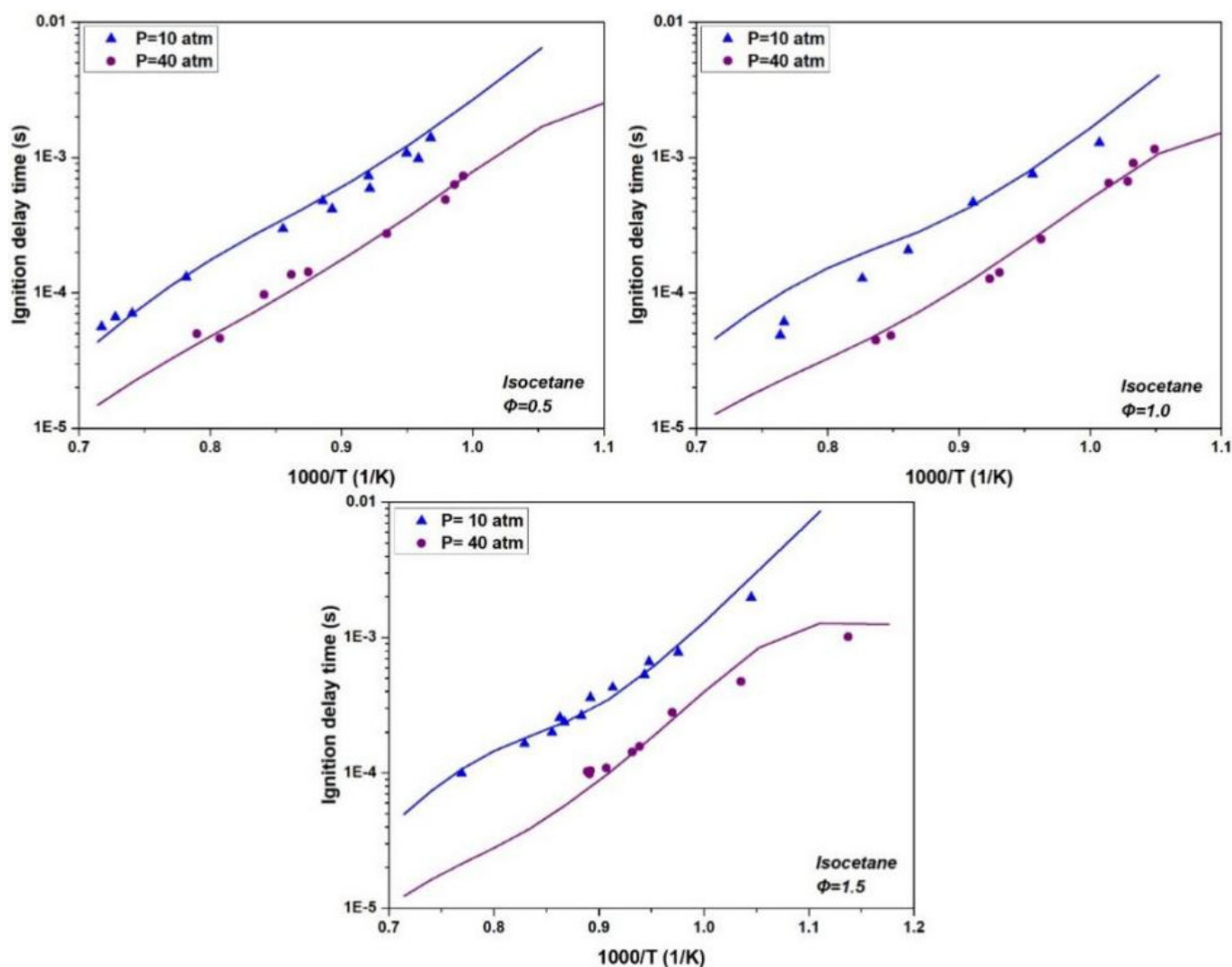


Figure 19. The measured (symbols [52]) and predicted IDTs (lines) of isocetane in the shock tube.

4.4.2. Species Concentration

Figure 20 shows the concentrations profiles of the major species produced during isocetane oxidation in a JSR [53]. The measurements were performed at a residence time of 1 s, under a pressure of 10 atm, and under three equivalence ratios (0.5, 1.0, and 2.0). It can be seen that the mechanism nicely predicts the consumption trend of isocetane under all conditions. The species mole fractions of H_2O and CO were also well predicted. The concentration of isocetane was overestimated in the high temperature range when $\Phi = 0.5$. For intermediate hydrocarbon products, the species profiles of CH_4 were not excellently reproduced by the mechanism, especially in the case of $\Phi = 1.0$.

4.5. Verifications of Jet Fuel

In this section, comparisons of ignition delay times, species mole fractions, and laminar flame speeds were further carried out for the newly developed JFS surrogate and the target jet fuel POSF-4658.

4.5.1. IDT

The shock tube experiments of jet fuel (POSF-4658) were conducted by S. Vasu et al. [8] and Wang et al. [54], as shown in Figure 21.

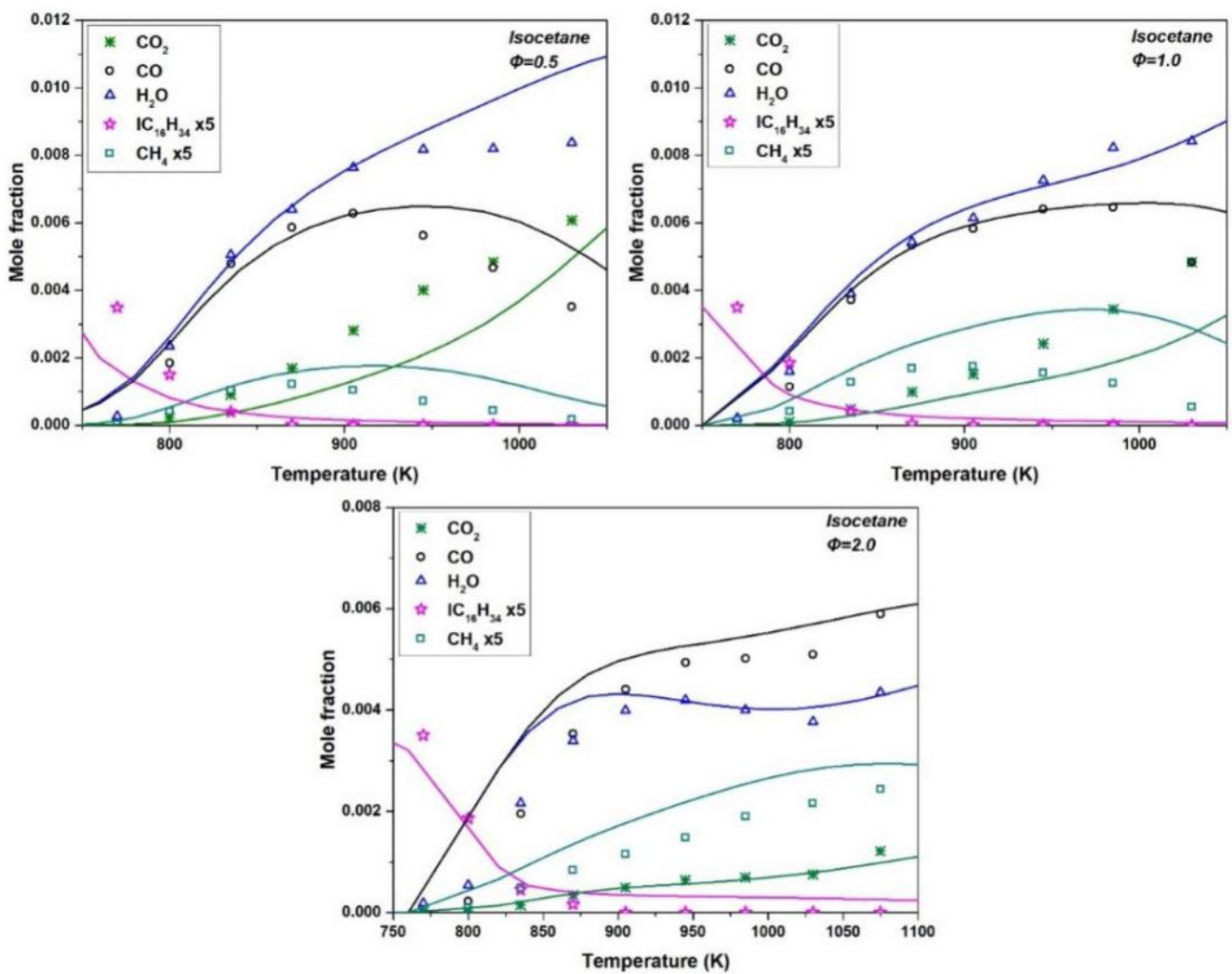


Figure 20. The measured (symbols [53]) and predicted (lines) major species profiles of isocetane in JSR experiments at different equivalence ratios.

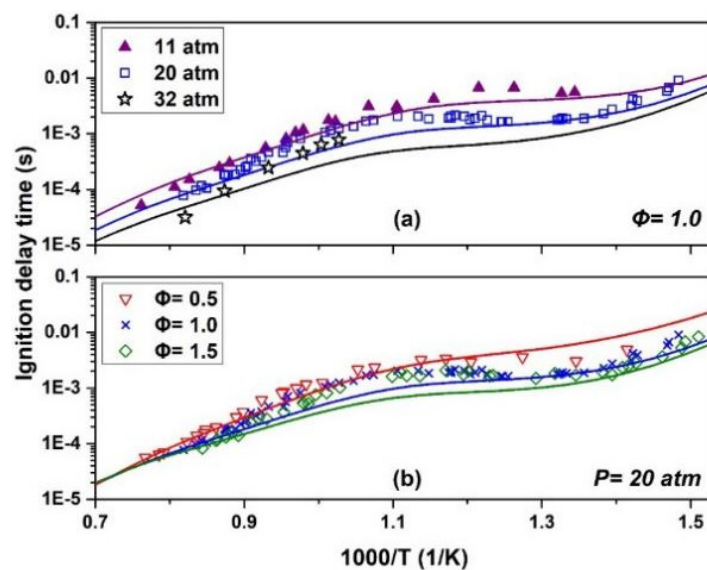


Figure 21. The comparisons between the determined and simulated IDTs of jet fuel under different (a) pressures and (b) equivalence ratios in a shock tube.

The comparisons between the determined and simulated IDTs of jet fuel at three pressures are exhibited in Figure 21a, while Figure 21b shows the results at three equivalence ratios: $\Phi = 0.5, 1.0,$ and 1.5 . The overall trends of the jet fuel IDTs were well reflected by the current mechanism, especially at low pressure and low equivalence ratios, which can be attributed to the reason that the H/C, CN, and LHV of the proposed JFS surrogate are similar to those of the target fuel. Although the predicted NTC region underwent a slight shift to the left under the conditions of $\Phi = 1.5$ and 20 atm pressure, the NTC behavior was satisfactorily captured via the developed mechanism. Furthermore, the maximum deviation between the predicted and measured IDTs is less than 0.001 s, and the small deviations between the predicted and measured IDTs can be attributed to two reasons: (1) Some reactions and species are removed from the reduced mechanism, which inevitably makes the mechanism unable to reproduce the measurements as well as the detailed mechanism. (2) There are still some differences between the properties of the JFS surrogate and the target fuel, which in turn influence the performance of the associated mechanism.

Figure 22 shows the comparison results between the measured IDTs and the IDTs predicted from the current JFS mechanism as well as the UM1 and UM2 mechanisms at $\Phi = 1.0$ and $p = 20$ atm. Both the surrogates UM1 and UM2 contain four components, and the components of UM2 and the current JFS surrogate are identical. The detailed mechanisms of UM1 and UM2 were developed by Kim et al. [15]. In general, all of the mechanisms give good predictions of the measured IDTs of jet fuels. The predictions still suffer some deviations in IDT against the experimental data within the intermediate temperature range (from 855 to 1030 K), even with the detailed mechanisms, and the maximum deviation between the predicted and measured IDTs is about 0.0015 s. It is worth mentioning that the reduced JFS mechanism has a comparable emulation capability to the UM1 and UM2 mechanisms, although the UM1 and UM2 mechanisms are much more detailed compared to the current mechanism.

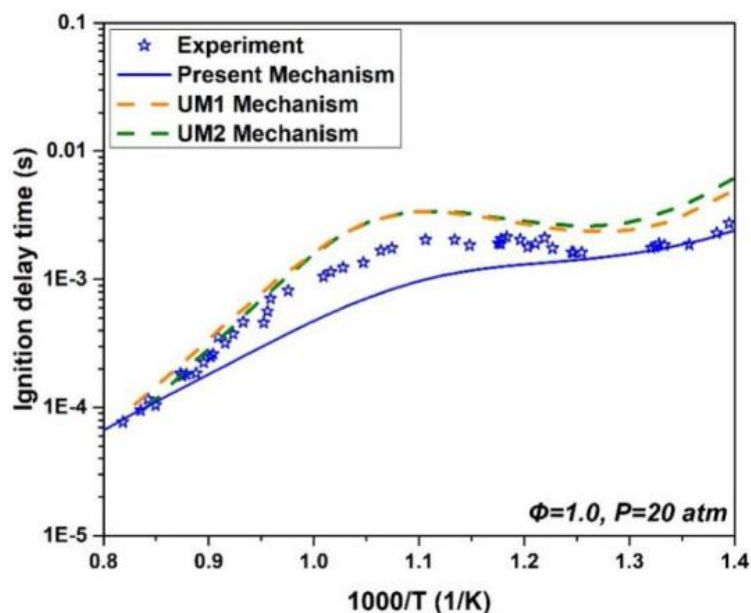


Figure 22. The comparison between the determined IDTs of jet fuel [12] and the simulated IDTs by the current mechanism, as well as the UM1 and UM2 mechanisms [15].

4.5.2. Species Concentration

Figure 23 shows the species profiles of the JFS surrogate in comparison with the experimental data determined in a shock tube at the temperature range of 890 K to 1680 K by Malewicky et al. [14].

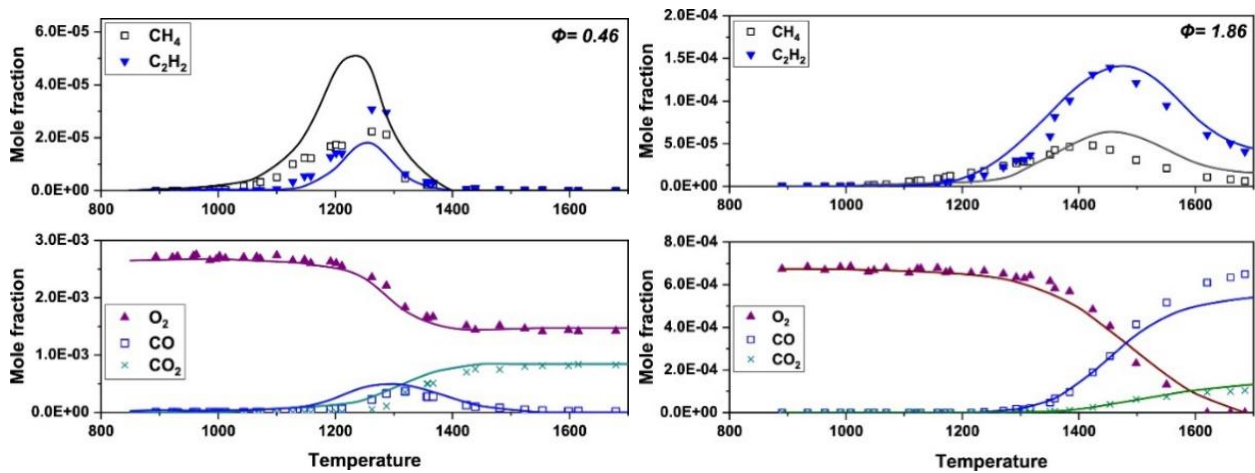


Figure 23. The measured and predicted species profiles of jet fuel. Symbols are the experimental data [14]; lines are the predictions made by the current mechanism.

The concentration profiles of CH_4 and C_2H_2 were well captured by the current mechanism, except for the slight overprediction for CH_4 at the lean condition ($\Phi = 0.46$), which implies that the mechanism is reliable in predicting the soot and PAH formulation in engine combustion. The decaying trend of O_2 and the increasing trend of CO_2 were both greatly reflected by the mechanism. As shown in Figure 23, the current mechanism also showed good performance in predicting the CO concentration except for a slight underestimation under the rich- and high-temperature condition (Figure 22b). Overall, the current mechanism exhibited a satisfactory prediction of the major species concentrations of the JFS surrogate, although the maximum deviation between the measurements and the predictions of CH_4 was larger than the measured value. In fact, similar deviations were also observed even using a detailed mechanism, as reported by Malewicki et al. [14].

4.5.3. Laminar Flame Speed

The comparison results between the simulated and measured laminar flame speeds is shown in Figure 24. The laminar flame speeds of jet fuel were measured by Dooley et al. [13] at atmospheric pressure and the unburned mixture temperatures of 400 K and 470 K. The predicted values showed a surprising consistency with the measurements, and the maximum discrepancy between them was less than 9.4%. According to Li et al. [55], H_2 , CO, and small hydrocarbons have decisive impacts on flame propagation; hence, great consistency can be attained through the adoption of a detailed C1/ H_2 /CO sub-mechanism in the current JFS mechanism.

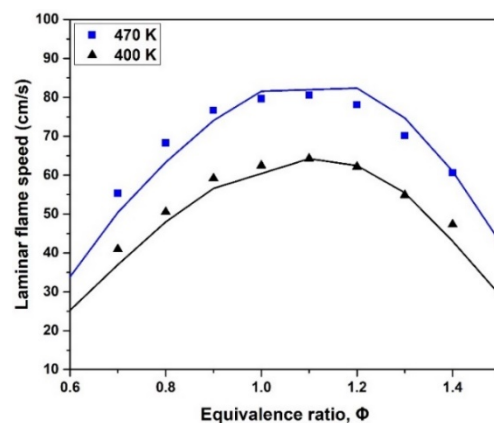


Figure 24. The comparison between the measured and predicted laminar flame speeds. Symbols represent the experimental data [13], lines are the values predicted by the current mechanism.

5. Conclusions

In this study, a new four-component jet fuel surrogate (n-dodecane/iso-octane/isocetane/decalin/toluene) was formulated with a property optimizer. The chemical and physical properties of the target jet fuel were considered during the formulation of the fuel surrogate. Compared to the previous-existing jet surrogates, the current jet fuel surrogate showed better performance in emulating the real jet fuel properties. The deviations in CN, TSI, LHV, and density are -0.35 , -1.29 , 0.87 , and 1.84 , which are extremely in a low level. The property deviations of MW (10.73%), viscosity (5.88%), and surface tension (8.71%) are slightly larger, but these remain within acceptable ranges.

A compact reduced kinetic mechanism consisting of 124 species and 590 reactions was proposed for the newly formulated surrogate. This mechanism is highly suitable for practical engine combustion simulations due to its reduced size. The mechanism is composed of four sub-mechanisms covering toluene, decalin, n-dodecane, and isocetane. It was systematically developed, starting from the C5–C16 reactions and transitioning to the C2–C4 reactions, followed by the H₂/O₂/C1 reactions, PAH reactions, and NO_x reactions. To validate the proposed mechanism, experimental data including ignition delay time (IDT), species concentrations, and laminar flame speeds were utilized, encompassing both the surrogate mixture and its individual components. The results demonstrated a favorable concordance between the proposed mechanism and the experimental data. The current mechanism could accurately capture the variations of the ignition delay time in the negative temperature coefficient (NTC) region. Consequently, the proposed mechanism emerges as a viable choice for effective utilization in practical engine simulations.

Author Contributions: Conceptualization, G.L.; methodology, G.L.; software, B.C.; validation, B.C.; data curation, C.Z.; writing—review and editing, L.C. (Longfei Chen); supervision, L.C. (Liuyong Chang). All authors have read and agreed to the published version of the manuscript.

Funding: This work was supported by the National Natural Science Foundations of China (Grant No. 52306181 and Grant No. 52306184) and National Key Research and Development Project of China (Grant No. 2022YFB2602002).

Institutional Review Board Statement: Not applicable.

Informed Consent Statement: Not applicable.

Data Availability Statement: The data used to support the findings of this study are available from the corresponding author upon request.

Conflicts of Interest: The authors declare no conflict of interest.

References

1. Wolfowitz, P. *DoD Management Policy for Energy Commodities and Related Services*; Department of Defense: Washington, DC, USA, 2004; p. 4140.25.
2. Sarathy, S.; Farooq, A.; Kalghatgi, G.T. Recent progress in gasoline surrogate fuels. *Prog. Energy Combust. Sci.* **2018**, *65*, 67–108. [[CrossRef](#)]
3. Zhen, X.; Yang, W.; Daming, L. An overview of the chemical reaction mechanisms for gasoline surrogate fuels. *Appl. Therm. Eng.* **2017**, *124*, 1257–1268. [[CrossRef](#)]
4. Kim, D.; Violi, A. Hydrocarbons for the next generation of jet fuel surrogates. *Fuel* **2018**, *228*, 438–444. [[CrossRef](#)]
5. Yu, W.; Zhao, F.; Yang, W.; Tay, K.; Xu, H. Development of an optimization methodology for formulating both jet fuel and diesel fuel surrogates and their associated skeletal oxidation mechanisms. *Fuel* **2018**, *231*, 361–372. [[CrossRef](#)]
6. Dooley, S.; Won, S.H.; Dryer, F.L. Chapter 10—Surrogate fuels. In *Computer Aided Chemical Engineering*; Faravelli, T., Manenti, F., Ranzi, E., Eds.; Elsevier: Amsterdam, The Netherlands, 2019; pp. 513–602.
7. Violi, A.; Yan, S.; Eddings, E.G.; Sarofim, A.F.; Granata, S.; Faravelli, T.; Ranzi, E. Experimental formulation and kinetic model for JP-8 surrogate mixtures. *Combust. Sci. Technol.* **2002**, *174*, 399–417. [[CrossRef](#)]
8. Vasu, S.S.; Davidson, D.F.; Hanson, R.K. Jet fuel ignition delay times: Shock tube experiments over wide conditions and surrogate model predictions. *Combust. Flame* **2008**, *152*, 125–143. [[CrossRef](#)]
9. Dagaut, P.; El Bakali, A.; Ristori, A. The combustion of kerosene: Experimental results and kinetic modelling using 1- to 3-component surrogate model fuels. *Fuel* **2006**, *85*, 944–956. [[CrossRef](#)]

10. Gokulakrishnan, P.; Gaines, G.; Currano, J.; Klassen, M.S.; Roby, R.J. Experimental and Kinetic Modeling of Kerosene-Type Fuels at Gas Turbine Operating Conditions. *J. Eng. Gas Turbines Power* **2006**, *129*, 655–663. [CrossRef]
11. Eddings, E.G.; Yan, S.; Ciro, W.; Sarofim, A.F. Formulation of a surrogate for the simulation of jet fuel pool fires. *Combust. Sci. Technol.* **2005**, *177*, 715–739. [CrossRef]
12. Dooley, S.; Won, S.H.; Chaos, M.; Heyne, J.; Ju, Y.; Dryer, F.L.; Kumar, K.; Sung, C.-J.; Wang, H.; Oehlschlaeger, M.A.; et al. A jet fuel surrogate formulated by real fuel properties. *Combust. Flame* **2010**, *157*, 2333–2339. [CrossRef]
13. Dooley, S.; Won, S.H.; Heyne, J.; Farouk, T.I.; Ju, Y.; Dryer, F.L.; Kumar, K.; Hui, X.; Sung, C.-J.; Wang, H.; et al. The experimental evaluation of a methodology for surrogate fuel formulation to emulate gas phase combustion kinetic phenomena. *Combust. Flame* **2012**, *159*, 1444–1466. [CrossRef]
14. Malewicki, T.; Gudiyella, S.; Brezinsky, K. Experimental and modeling study on the oxidation of Jet A and the n-dodecane/iso-octane/n-propylbenzene/1, 3, 5-trimethylbenzene surrogate fuel. *Combust. Flame* **2013**, *160*, 17–30. [CrossRef]
15. Kim, D.; Martz, J.; Violi, A. A surrogate for emulating the physical and chemical properties of conventional jet fuel. *Combust. Flame* **2014**, *161*, 1489–1498. [CrossRef]
16. Verhelst, S.; Turner, J.W.; Sileghem, L.; Vancoillie, J. Methanol as a fuel for internal combustion engines. *Prog. Energy Combust. Sci.* **2019**, *70*, 43–88. [CrossRef]
17. Bae, C.; Kim, J. Alternative fuels for internal combustion engines. *Proc. Combust. Inst.* **2017**, *36*, 3389–3413. [CrossRef]
18. Yu, W.; Yang, W.; Tay, K.; Zhao, F. An optimization method for formulating model-based jet fuel surrogate by emulating physical, gas phase chemical properties and threshold sooting index (TSI) of real jet fuel under engine relevant conditions. *Combust. Flame* **2018**, *193*, 192–217. [CrossRef]
19. McDaniel, A.; Dickerson, T.; Luning-Prak, D.; Hamilton, L.; Cowart, J. *A Technical Evaluation of New Renewable Jet and Diesel Fuels Operated in Neat Form in Multiple Diesel Engines*; SAE Technical Paper; SAE International: Warrendale, PA, USA, 2016. [CrossRef]
20. Murphy, M.J.; Taylor, J.D.; McCormick, R.L. *Compendium of Experimental Cetane Number Data*; National Renewable Energy Laboratory: Golden, CO, USA, 2004.
21. *DIPPR Project 801—Full Version*; Design Institute for Physical Property Research/AIChE: New York, NY, USA, 2012.
22. Mensch, A.; Santoro, R.; Litzinger, T.; Lee, S.-Y. Sooting Characteristics of Surrogates for Jet Fuels. *Combust. Flame* **2010**, *157*, 1097–1105. [CrossRef]
23. Gill, R.J.; Olson, D.B. Estimation of Soot Thresholds for Fuel Mixtures. *Combust. Sci. Technol.* **1984**, *40*, 307–315. [CrossRef]
24. Grunberg, L.; Nissan, A.H. Mixture Law for Viscosity. *Nature* **1949**, *164*, 799–800. [CrossRef]
25. Poling, B.E.; Thomson, G.H.; Friend, D.G.; Rowley, R.L.; Wilding, W.V. *Perry's Chemical Engineers' Handbook*; McGraw-Hill Publishing: New York, NY, USA, 2008.
26. Hugill, J.; Van Welsenens, A.J. Surface tension: A simple correlation for natural gas+ condensate systems. *Fluid Phase Equilibria* **1986**, *29*, 383–390. [CrossRef]
27. Agosta, A.; Cernansky, N.; Miller, D.; Faravelli, T.; Ranzi, E. Reference components of jet fuels: Kinetic modeling and experimental results. *Exp. Therm. Fluid Sci.* **2004**, *28*, 701–708. [CrossRef]
28. Wang, H.; Yao, M.; Yue, Z.; Jia, M.; Reitz, R.D. A reduced toluene reference fuel chemical kinetic mechanism for combustion and polycyclic-aromatic hydrocarbon predictions. *Combust. Flame* **2015**, *162*, 2390–2404. [CrossRef]
29. Dagaut, P.; Ristori, A.; Frassoldati, A.; Faravelli, T.; Dayma, G.; Ranzi, E. Experimental and semi-detailed kinetic modeling study of decalin oxidation and pyrolysis over a wide range of conditions. *Proc. Combust. Inst.* **2013**, *34*, 289–296. [CrossRef]
30. Yu, L.; Wu, Z.; Qiu, Y.; Qian, Y.; Mao, Y.; Lu, X. Ignition delay times of decalin over low-to-intermediate temperature ranges: Rapid compression machine measurement and modeling study. *Combust. Flame* **2018**, *196*, 160–173. [CrossRef]
31. Chang, Y.; Jia, M.; Liu, Y.; Li, Y.; Xie, M.; Yin, H. Application of a Decoupling Methodology for Development of Skeletal Oxidation Mechanisms for Heavy n-Alkanes from n-Octane to n-Hexadecane. *Energy Fuels* **2013**, *27*, 3467–3479. [CrossRef]
32. Fan, W.; Jia, M.; Chang, Y.; Xie, M. Understanding the relationship between cetane number and the ignition delay in shock tubes for different fuels based on a skeletal primary reference fuel (n-hexadecane/iso-cetane) mechanism. *Energy Fuels* **2015**, *29*, 3413–3427. [CrossRef]
33. CHEMKIN-PRO RJI, San Diego, CA. 15112, Reaction Design. 2011. Available online: <https://www.ansys.com/products/fluids/ansys-chemkin-pro> (accessed on 6 July 2023).
34. Wang, L.; Wu, Z.; Ahmed, A.; Badra, J.A.; Sarathy, S.M.; Roberts, W.L.; Fang, T. Autoignition of direct injection spray of light naphtha, primary reference fuels, gasoline and gasoline surrogate. *Energy* **2019**, *170*, 375–390. [CrossRef]
35. Shen, H.-P.S.; Vanderover, J.; Oehlschlaeger, M.A. A shock tube study of the autoignition of toluene/air mixtures at high pressures. *Proc. Combust. Inst.* **2009**, *32*, 165–172. [CrossRef]
36. Kukkadapu, G.; Kang, D.; Wagnon, S.W.; Zhang, K.; Mehl, M.; Monge-Palacios, M.; Wang, H.; Goldsborough, S.S.; Westbrook, C.K.; Pitz, W.J. Kinetic modeling study of surrogate components for gasoline, jet and diesel fuels: C7-C11 methylated aromatics. *Proceeding Combust. Inst.* **2019**, *37*, 521–529. [CrossRef]
37. Pitz, W.J.; Mueller, C.J. Recent progress in the development of diesel surrogate fuels. *Prog. Energy Combust. Sci.* **2019**, *37*, 330–350. [CrossRef]
38. Li, Y.; Cai, J.; Zhang, L.; Yuan, T.; Zhang, K.; Qi, F. Investigation on chemical structures of premixed toluene flames at low pressure. *Proceeding Combust. Inst.* **2011**, *33*, 593–600. [CrossRef]

39. Yuan, W.; Li, Y.; Dagaut, P.; Yang, J.; Qi, F. Investigation on the pyrolysis and oxidation of toluene over a wide range conditions. I. Flow reactor pyrolysis and jet stirred reactor oxidation. *Combust. Flame* **2015**, *162*, 3–21. [[CrossRef](#)]
40. Zhao, F.; Yang, W.; Zhou, D.; Yu, W.; Li, J.; Tay, K.L. Numerical modelling of soot formation and oxidation using phenomenological soot modelling approach in a dual-fueled compression ignition engine. *Fuel* **2017**, *188*, 382–389. [[CrossRef](#)]
41. Davis, S.; Wang, H.; Breinsky, K.; Law, C.K. Laminar flame speeds and oxidation kinetics of benene-air and toluene-air flames. Conference Laminar flame speeds and oxidation kinetics of benene-air and toluene-air flames. *Symp. (Int.) Combust.* **1996**, *26*, 1025–1033. [[CrossRef](#)]
42. Johnston, R.; Farrell, J. Laminar burning velocities and Markstein lengths of aromatics at elevated temperature and pressure. *Proc. Combust. Inst.* **2005**, *30*, 217–224. [[CrossRef](#)]
43. Zhu, Y.; Davidson, D.; Hanson, R. Pyrolysis and oxidation of decalin at elevated pressures: A shock-tube study. *Combust. Flame* **2014**, *161*, 371–383. [[CrossRef](#)]
44. Oehlschlaeger, M.A.; Shen, H.-P.S.; Frassoldati, A.; Pierucci, S.; Ranzi, E. Experimental and Kinetic Modeling Study of the Pyrolysis and Oxidation of Decalin. *Energy Fuels* **2009**, *23*, 1464–1472. [[CrossRef](#)]
45. Curran, H.; Gaffuri, P.; Pitz, W.; Westbrook, C. A Comprehensive Modeling Study of n-Heptane Oxidation. *Combust. Flame* **1998**, *114*, 149–177. [[CrossRef](#)]
46. Zeng, M.; Li, Y.; Yuan, W.; Li, T.; Wang, Y.; Zhou, Z.; Zhang, L.; Qi, F. Experimental and kinetic modeling study of laminar premixed decalin flames. *Combust. Flame* **2017**, *36*, 1193–1202. [[CrossRef](#)]
47. Li, B.; Zhang, H.; Egolfopoulos, F.N. Laminar flame propagation of atmospheric iso-cetane/air and decalin/air mixtures. *Combust. Flame* **2014**, *161*, 154–161. [[CrossRef](#)]
48. Vasu, S.; Davidson, D.; Hong, Z.; Vasudevan, V.; Hanson, R. n-Dodecane oxidation at high-pressures: Measurements of ignition delay times and OH concentration time-histories. *Proc. Combust. Inst.* **2009**, *32*, 173–180. [[CrossRef](#)]
49. Shen, H.-P.S.; Steinberg, J.; Vanderover, J.; Oehlschlaeger, M.A. A Shock Tube Study of the Ignition of n-Heptane, n-Decane, n-Dodecane, and n-Tetradecane at Elevated Pressures. *Energy Fuels* **2009**, *23*, 2482–2489. [[CrossRef](#)]
50. Haylett, D.R.; Davidson, D.F.; Hanson, R.K. Ignition delay times of low-vapor-pressure fuels measured using an aerosol shock tube. *Combust. Flame* **2012**, *159*, 552–561. [[CrossRef](#)]
51. Kumar, K.; Sung, C.J. Laminar flame speeds and extinction limits of preheated n-decane/O₂/N₂ and n-dodecane/O₂/N₂ mix-tures. *Combust. Flame* **2007**, *151*, 209–224. [[CrossRef](#)]
52. Oehlschlaeger, M.A.; Steinberg, J.; Westbrook, C.K.; Pitz, W.J. The autoignition of iso-cetane at high to moderate temperatures and elevated pressures: Shock tube experiments and kinetic modeling. *Combust. Flame* **2009**, *156*, 2165–2172. [[CrossRef](#)]
53. Dagaut, P.; Hadj-Ali, K. Chemical Kinetic Study of the Oxidation of Isocetane (2,2,4,4,6,8,8-Heptamethylnonane) in a Jet-stirred Reactor: Experimental and Modeling. *Energy Fuels* **2009**, *23*, 2389–2395. [[CrossRef](#)]
54. Wang, H.; Oehlschlaeger, M.A. Autoignition studies of conventional and Fischer–Tropsch jet fuels. *Fuel* **2012**, *98*, 249–258. [[CrossRef](#)]
55. Li, J.; Zhao, Z.; Kazakov, A.; Chaos, M.; Dryer, F.L.; Scire, J.J., Jr. A comprehensive kinetic mechanism for CO, CH₂O, and CH₃OH combustion. *Int. J. Chem. Kinet.* **2007**, *39*, 109–136. [[CrossRef](#)]

Disclaimer/Publisher’s Note: The statements, opinions and data contained in all publications are solely those of the individual author(s) and contributor(s) and not of MDPI and/or the editor(s). MDPI and/or the editor(s) disclaim responsibility for any injury to people or property resulting from any ideas, methods, instructions or products referred to in the content.